Journal of Bio- and Tribo-Corrosion (2023) 9:80
https://doi.org/10.1007/s40735-023-00796-z

Experimental and Theoretical Approach of Evaluating Chitosan Ferulic Acid Amide as an Effective Corrosion Inhibitor

S. J. Hepziba Magie Jessima[1] · S. Subhashini[2] · Avni Berisha[3] · Valbonë Mehmeti[4] · Subramanian Sathy Srikandan[5]

Received: 3 May 2023 / Revised: 18 August 2023 / Accepted: 2 September 2023 / Published online: 6 October 2023

Abstract

Phenolic acid grafted chitosan has widespread drug delivery applications, as bio adsorbent, packing material, etc., due to its excellent antioxidant and antimicrobial properties. However, for the first time, the anticorrosive efficiency of ferulic acid modified chitosan has been investigated. The prepared chitosan derivative is characterized using spectral methods, thermal analytical methods, surface charge, and particle size analysis. The evaluation of corrosion inhibition potential showed a highest value of 95.96% at 303 K. Thermodynamic activation and adsorption parameters endorse a mixed adsorption process involving an initial electrostatic interaction followed by chemisorption. Electrochemical studies gave results which agreed well with the gravimetric studies. Surface morphological studies were performed using contact angle measurements, FESEM, EDAX, AFM, optical profilometric and UV spectral techniques. Computational studies involving quantum chemical calculations, Monte Carlo and molecular dynamic simulation studies, and radial distribution function analysis are further done to validate the experimental results.

Graphical Abstract

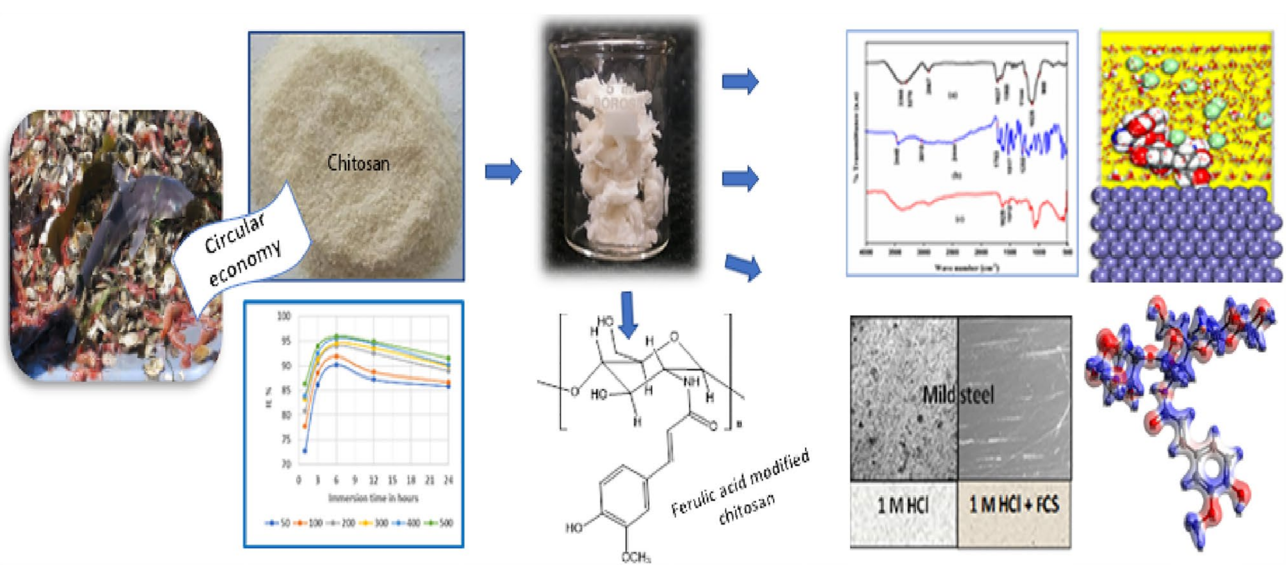

Keywords Modified chitosan · Mild steel · Corrosion inhibitors · EIS · Monte Carlo and molecular dynamic simulation

Extended author information available on the last page of the article

1 Introduction

The acid treatment of metals, namely acid pickling, descaling, etching, etc., renders the metal surface free from stain, scale, rust, and other impurities. However, this action exposes the clean, bare metal more to the aggressive medium resulting in an increased metal dissolution. Therefore, corrosion inhibitors are used as additives in the cleaning acids. These additives mitigate corrosion by adsorbing themselves on the metal surface, forming a protective film that prevents the metal surface from being exposed to the aggressive environment [1, 2]. The use of inhibitors is economical and compatible compared to other mitigation techniques. Besides, it allows the use of low-grade carbon steel in the place of high-cost alloys [3]. There are numerous corrosion inhibitors tested and proven, but only a few are employed in practice. This observation reveals that in addition to protection, certain other factors such as cost-effectiveness, eco-friendly, non-toxic nature, ready availability, and compatibility in combating corrosion also matters. Polymers can act as effective corrosion inhibitors due to their inherent stability, ability to form complexes that can blanket the metal surface, and multiple binding sites that help in slower desorption.

Many of the natural polymers such as natural gums [4, 5], pectin [6–8], derivatives of cellulose [9–12], starch [13–15], carrageen [16, 17], alginates [18, 19], polysaccharide from maca (*Lepidium meyenii*) root extract [20], biomolecules-based expired drugs [21] expired herbal drug bearing glycosides and polysaccharides [22] have been evaluated as potential corrosion inhibitors for different metals in acidic and neutral solutions.

Chitosan derived by *N*-deacetylation process of chitin, the second most abundant polysaccharide on earth next to cellulose is found to be a promising biopolymer in the field of corrosion inhibition. Chitosan, the only cationic natural polysaccharide is composed of β-(1 → 4)-linked D-glucosamine and *N*-acetyl-D-glucosamine units. The presence of reactive poly hydroxyl groups and free amine groups make it an efficient functional material that can be exploited in various applications [23]. These functional groups can serve as potential adsorption sites to interact effectively with the metal surface. In addition, the ecofriendliness of chitosan has driven the research studies towards the evaluation of the corrosion inhibition efficiency of chitosan for different metals in different aggressive environment. Vorster filed a patent on chitosan as relatively cheap and non-toxic corrosion inhibitor for ferrous metals in acid chlorides and acid sulphates [24]. Though the evaluated inhibition efficiency of chitosan was promising, the drawback of low water solubility limited its application as corrosion inhibitor. Hence chitosan was chemically modified to enhance its solubility in water so that it can be used as corrosion inhibitor in any pH conditions.The hydroxyl group at the C-6 position and amino group at the C-2 position in chitosan are potential avenues for modification through chemical reactions even under mild conditions [25]. Chitosan-based thiosemicarbazide, thiocarbohydrazide, and Schiff bases also proved to be efficient green corrosion inhibitors [26, 27]. Studies on chitosan and its derivatives reveal its efficacy as potential green corrosion inhibitors. Polyaniline chitosan demonstrated a corrosion inhibition efficiency of 84.78% for Q_{235} mild steel in the acid medium [28]. PEG crosslinked chitosan showed an excellent corrosion inhibition efficiency of 93.9% for mild steel in sulphamic acid [29]. Amylose acetate blended carboxymethyl chitosan records an anticorrosive potential of 97.65% against mild steel in the acid medium [30]. Sodium lauryl sulfate modified chitosan and disodium EDTA functionalized chitosan revealed an inhibition efficiency of 96.44% and 96.63%, respectively [31, 32]. Synthetic chitosan derivatives such as *N*-phenylthiourea chitosan and *N*-phenyl-*O*-benzylthiourea chitosan showed a corrosion inhibiton efficiency of 98.4% and 98.5%, respectively, at the concentration of 100 mg/L for carbon steel [33]. L-arginine grafted chitosan was found to show an inhibition efficiency of 91.4% for mild steel in 0.5 M HCl [34]. Chitosan derivatives are proved to be excellent corrosion mitigators of other metals such as magnesium alloy in saline medium, copper in 1 M HCl, aluminium in sodium chloride solution [35–37].

The literature survey also reveals the various attempts to relate the antioxidant properties with that of the anticorrosive behavior in different plant extracts and organic compounds. Sher and Voevoda made a comparative study of antioxidant and anticorrosive properties of metal dialkyl- and diaryldithiophosphates [38]. Boujakhrout et al. studied the antioxidant activity and corrosion inhibitive behavior of Garcinia cola seeds and brazilian plant extracts [39]. Hussin et al. investigated derivatives of (2Z,4E)-3-hydroxy-1-(2-hydroxyphenyl)-5-phenylpenta-2,4-die-1-ones for their antioxidant activity and corrosion inhibition potential [40]. Mayakrishnan et al. evaluated antioxidant and anticorrosion properties of Epipremnum aureum leaves [41]. While Vorobyova et al. concluded that increase in total antioxidants in plant extracts can increase the corrosive inhibition [42]. This survey was done to analyze whether antioxidative properties can serve as a predictive index to evaluate the corrosion inhibition efficiency. Therefore, the present study targets the preparation of a water-soluble chitosan modified corrosion inhibitor with excellent antioxidant properties. By employing chitosan from the seafood waste, the dire need of the hour, namely practicing circular economy, has been realized in this research work.

Scheme 1 Preparation of FCS

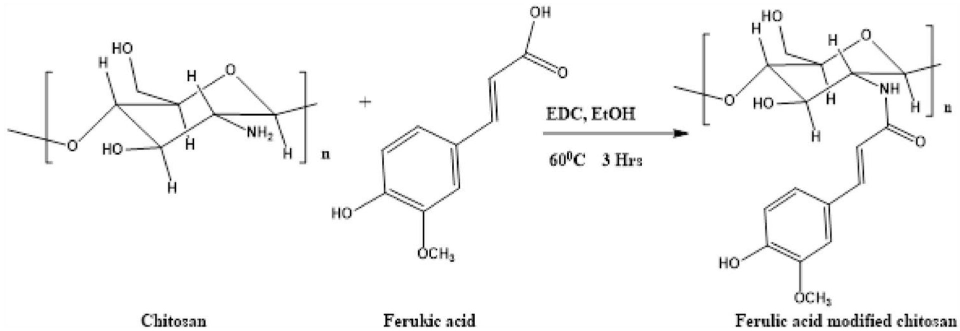

In the present investigation, ferulic acid modified chitosan (FCS) was prepared using the method reported earlier [43] with slight modification and was characterized using different techniques. FCS plays a significant role in several biomedical applications, and for the first time, its application in the field of corrosion is explored in the present study. The corrosion mitigation efficiency of FCS was assessed using the gravimetric method and electrochemical studies. Surface studies serve as evidence for the mitigation potential of the inhibitor [31]. Theoretical studies were done to validate the experimental results.

2 Experimental

2.1 Instrumentation

The functional group characterization of FCS was done using ATR-FTIR (Shimadzu IRSpirit), UV–visible (Shimadzu UV-1800), and proton NMR (Bruker 400 MHz NMR) spectral studies. Thermogravimetric and differential scanning calorimetric curves were recorded (STA-6000 from Perkin Elmer) to analyze the temperature response. Malvern Zeta sizer (ZEN 3600) was employed to study the particle charge and size analysis.

Gamry Reference—600 instrument was employed for the electrochemical studies and Echemanalyst software for interpreting the experimental results.

Surface morphology studies of the metal samples were done to relate the decrease in metal dissolution with the inhibitor film formation. The contact angle analyzer, Phoenix 300 Plus model, was used for the contact angle measurement. Carl Zeiss Sigma V Field Emission Scanning Electron Microscope was employed for SEM and EDAX analyses. Atomic force microscope (NTDMT model) and optical profilometer (ZETA-20 model), engaged for surface topography and roughness studies. Images in the optical profilometer captured using a ×20 magnification lens. Zeta 3D software is used for the analysis of the images.

2.2 Chemicals and Reagents

Chitosan (75% deacetylated) from Sigma-Aldrich, ferulic acid (minimum assay of 99.0%) from Hi-Media Laboratories Pvt. Ltd. the carbodiimide coupling reagent (EDC) and doubly distilled water from Sisco Research Laboratories Pvt. Ltd. were procured for the present research. Analar grade concentrated hydrochloric acid, acetone, ethanol, methanol were used for the investigation. Chitosan was further washed with boiling water, followed by methanol, and dried in a vacuum desiccator [44].

2.3 Mild Steel Metal Samples

Mild steel samples were cut into strips of $5 \times 1 \times 0.2$ cm dimension and 1×1 cm dimension for weight loss and electrochemical studies. The metal samples were polished with a buff wheel, abraded with fine emery sheets, cleaned, and degreased before storing in the desiccator for further use.

2.4 Preparation of Corrosion Inhibitor

Chitosan in 25 ml of 0.25 M hydrochloric acid was stirred overnight at room temperature. An equal amount of ferulic acid is added to the EDC coupling reagent in 10 ml of absolute ethanol. The mixture is then slowly transferred to the chitosan solution placed on a magnetic stirrer maintained at 60 °C. The stirring was continued for 3 h, and the white precipitate obtained was washed with acetone, then kept in a desiccator for drying. Scheme 1 display the chemical reaction involved in the preparation of the modified chitosan.

2.5 Assessment of Anticorrosive Performance of FCS

2.5.1 Gravimetric Studies

Gravimetric studies was carried out based on standard ASTM procedure (ASTM G1-03) [45]. Mild steel specimen of composition Fe-94.43%, C-0.175%, Si-0.258%, Mn-0.456%, P-0.013%, S-0.007%, Cr-0.983%, Mo-0.195%, Ni-3.306%, Al-0.023%, Cu-0.078%, Ti-0.004%, V-0.011%, W-0.040%, Pb-0.005%, N-0.015%, Nb-0.006% was used for the present investigation. Preweighed metal samples in triplicates were held in suitable glass hooks and immersed in 100 ml beakers containing 0 to 500 ppm concentration of FCS inhibitor in 1 M HCl [46]. The immersion periods chosen for the present study include ½, 1, 3, 6, 12, and 24 h at 303 K. After the stipulated immersion periods, the samples were removed, washed thoroughly with water, and placed in the desiccator. The metal samples are weighed again to note the weight loss. The same procedure was repeated for the temperature studies done at 303, 313, 323, 333, and 343 K for an immersion period of half an hour. Both the immersion and temperature studies were performed in triplicates under aerated and unstirred conditions.

The inhibition efficiency (η_{CI}) of FCS against corrosion was calculated using Eq. 1 and corrosion rate (K_{CR}) using Eq. 2.

$$\eta_{CI} = \frac{W_b - W_i}{W_b} \times 100 \tag{1}$$

$$K_{CR}(\text{mpy}) = \frac{3.45 \times 10^6 \times \text{weight loss}}{\text{DAT}}, \tag{2}$$

where w_b and w_i represent the weight loss of the metal samples when exposed to 1 M hydrochloric acid and FCS solution, respectively. D is the metal density in g/cm^3, A is the area of the metal samples in cm^2 and T indicates the exposure period in hours.

2.5.2 DC and AC Electrochemical Measurements

Tafel, linear polarization resistance, and AC impedance studies were carried out at room temperature under aerated and unstirred conditions using Gamry Reference 600 instrument. Mild steel sample was employed as the working electrode, stable and robust saturated calomel electrode as reference electrode, and platinum electrode as an auxiliary to complete the cell circuit. The electrochemical impedance spectroscopic studies were performed at a frequency range of 100 kHz to 0.01 Hz with 10 mV amplitude as AC signal at steady-state open circuit potential. Echemanalyst software interpreted the experimental results. Tafel polarization curves were obtained by applying a sweeping potential of + 250 mV anodically and − 250 mV cathodically versus the open circuit potential at 0.1666 mV/s scan rate as per ASTM G59-97 (2014) [47]. Mostly 1 mV/s is used as scan rate for potentiodynamic polarisation measurements of corrosion rates as was found in the literature. However, the experiment was performed at the standard scan rate of 0.1667 mV according to ASTM recommendations, although a faster scan rate of 1 mV/s is permitted [48–54]. Low scan rate as recommended by ASTM can produce high quality and reliable output, however is a time-consuming process [55]. Therefore, scan rates in the order of 0.5 mV/s, 1 mV/s and 1.67 mV/s are employed which also is found to give good results [56–61]. The scan rate is an important parameter in the polarisation experiment as the rapid scan rate results in the incomplete charge transfer within the interface of the working electrode, while the lowest scan rate may cause irreversible changes to the interface structure of the corroding system leading to erroneous results [55]. The linear polarization resistance measurements were made at ± 20 mV vs. OCP and 0.5 mV/s scan rate [62, 63].

The percentage of inhibition efficiency of the FCS inhibitor is calculated using i_{corr} values from Tafel studies, LPR values from linear polarisation studies, and R_p values from impedance studies employing the following equations.

$$IE_T\,(\%) = \left(\frac{I_{corr_0} - I_{corr_{inh}}}{I_{corr_0}}\right) \times 100 \tag{3}$$

$$IE_{LPR}\,(\%) = \left(\frac{\text{LPR}_{inh} - \text{LPR}_0}{Rp_{inh}}\right) \times 100 \tag{4}$$

$$IE_{Rp}\,(\%) = \left(\frac{Rp_{inh} - Rp_0}{Rp_{inh}}\right) \times 100 \tag{5}$$

where I_{corr_0} and $I_{corr_{inh}}$, LPR$_0$ and LPR$_{inh}$, R_{P_0} and $R_{P_{inh}}$ represent the corrosion current density, linear polarisation resistance, and polarization resistance obtained when the electrolyte solution was 1 M HCl and FCS, respectively

2.6 Theoretical Studies

2.6.1 Quantum Chemical Calculations

Quantum chemical calculations were done using density functional theory employing Gaussian 09 software in the framework of the B3LYP/6 − 31 + G (d, p) basis set. Theoretical parameters were calculated for the optimized molecular geometry of neutral and protonated FCS [64]. The Mulliken charges generated aided to locate the potential sites of protonation, and the most favourable protonation site was decided by calculating the proton affinity values for each potential site. According to Koopman's theorem, the following parameters are related to the energy of the frontier orbitals E_{HOMO} and E_{LUMO} by Eqs. S1 and S2.

According to Mulliken, the electronegativity (χ) is the average value of ionization potential and electron affinity represented by Eq. S3. Similarly, the global hardness (η) is calculated using the Eq. S4.

η is related to the energy gap between the frontier molecular orbitals. The lesser the energy gap, the more is the softness, and the greater is its chemical reactivity.

According to Parr et al., the electrophilicity index (ω) is the natural tendency of a species to accept electrons. The electrophilicity index (ω) can be calculated using the Eq. S5.

The quantum parameter ΔN is used to evaluate the altitude of the transferred electrons and is represented by the Eq. S6.

2.6.2 Monte Carlo and Molecular Dynamic Simulation Details

The evaluation of the interaction between the Fe (110) surface and the inhibitor molecule (FCS) throughout Monte Carlo (MC) and Molecular dynamic (MD) simulation is performed in the simulated corrosion medium by the use of a seven atom-thick layer unit cell of Fe (110) surface. The slab size used in these calculations was: 24.842 Å × 24.842 Å × 12.533 Å with a 25 Å vacuum layer. This box is filled with 550 water molecules/1 inhibitor molecule (in neutral or protonated state)/10 hydronium + 10 chloride ions [65].

MD was attained using the NVT at 298 K over a simulation time of 300 ps (using a 1 fs time step and 0.5 ns simulation time) [66–69]. The temperature control is attained via the Berendsen thermostat [70]. The recurrently COMPASSII forcefield used in corrosion studies was used for the MC (Monte Carlo) and MD (Molecular Dynamic) [71–74]. The Radial Distribution Function (RDF) analysis is implemented on the complete trajectory of the MD [31, 73, 75].

3 Results and Discussion

3.1 Spectral Characterization, Thermal Stability, and Zeta Potential Analysis of FCS

Comparative infrared spectra of (a) chitosan biopolymer, (b) ferulic acid, and (c) FCS is displayed in Fig. 1. The chitosan spectrum shows absorption bands at 3270–368 cm^{-1} arising due to N–H and O–H stretching vibrations. This band also includes intramolecular hydrogen bond characteristic of polysaccharides. The symmetric and asymmetric stretching of C–H bonds occur at 2911 and 2867 cm^{-1}. The C=O and C–N stretching vibrations of the *N*-acetyl group are found at 1637 cm^{-1} and 1317 cm^{-1}. The absorbance band found at 1568 cm^{-1} is due to N–H bending vibrations of the primary amine. CH_2 bending vibrations and CH_3 symmetrical deformations are identified at 1420 cm^{-1} and 1381 cm^{-1}, respectively. IR peaks at 1144 cm^{-1}, 1059 cm^{-1} and 1025 cm^{-1} corresponds to the C–O–C bridge and C–O asymmetric stretching. The C–H bending vibrations of out of plane of the monosaccharide ring correspond to the peak at 900 cm^{-1} [76]. Ferulic acid has the following characteristic peaks, namely O–H stretching at 3448 cm^{-1} and C–H stretching at 2911–3015 cm^{-1}, C=O stretching of the carboxyl group at 1703 cm^{-1}, C=C of the aromatic ring at 1517 cm^{-1}, and C–O stretching of the carboxylic group at 1272 cm^{-1} [77]. The new peak at 1512 cm^{-1} corresponds to C=C of the aromatic ring that serves as evidence for FCS formation. The intensity of C=O and N–H stretching bands of the amide group found at 1625 cm^{-1}, and 1553 cm^{-1} is also increased. The increased peak intensity at 2926 cm^{-1} can be attributed

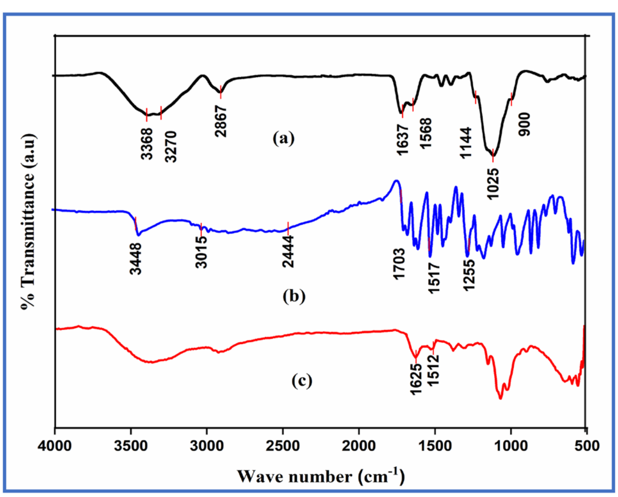

Fig. 1 Comparative IR spectrum of (**a**) chitosan biopolymer, (**b**) ferulic acid and (**c**) FCS

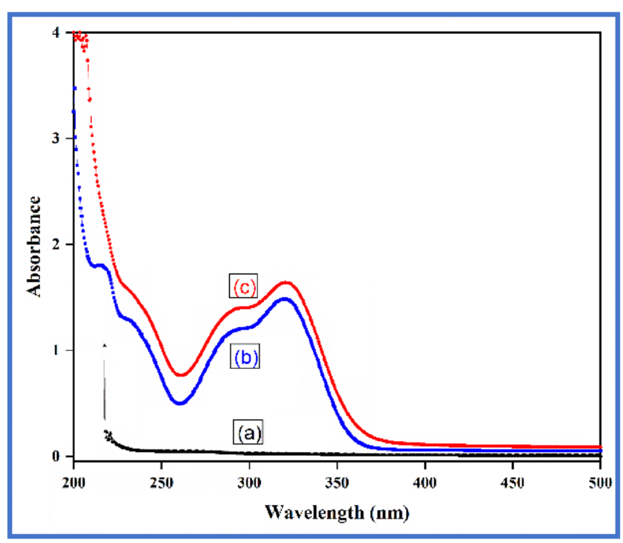

Fig. 2 Comparative UV spectrum of (**a**) chitosan, (**b**) ferulic acid, and (**c**) FCS

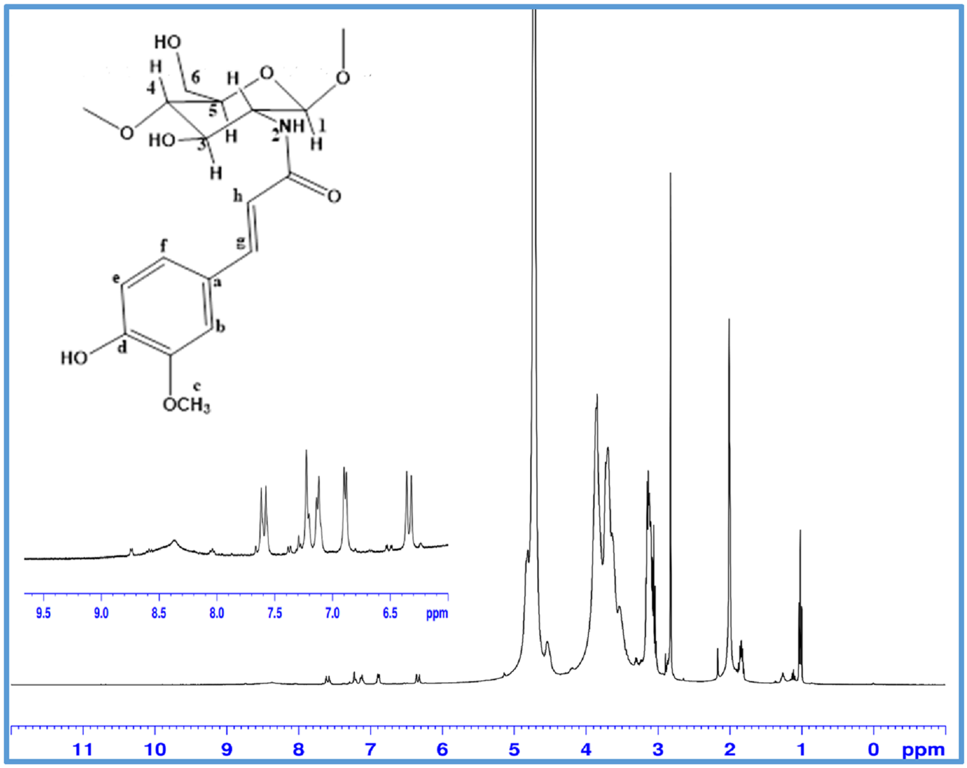

Fig. 3 NMR spectrum of FCS inhibitor

to C–H stretching. The disappearance of the N–H absorption peak of the primary amine at 1589 cm^{-1} further supports the grafting process [43, 78]. There is no IR peak at 1730 cm^{-1} that confirms the absence of ester formation.

Figure 2 displays the UV–visible spectra of chitosan biopolymer, ferulic acid, and FCS. Chitosan in 1% acetic acid is found to give no absorption peak in the entire spectral range from 250 to 400 nm. An ethanolic solution of ferulic acid shows an absorbance maximum at 290 nm and 321 nm. FCS in 1 M HCl solution shows the same absorbance maxima at 321 nm that supports chitosan ferulic acid amide [43, 79]. Some literature studies also have highlighted redshift for ferulic acid grafted chitosan [80].

The chemical structure of the FCS inhibitor is further characterized using H^1 NMR spectra portrayed in Fig. 3. The D_2O solvent peak is found at 4.8 ppm, and the proton signals at 3.8 ppm, 6.3 ppm, and 7.6 ppm correspond to $-OCH_3$ and methine protons $CH_{(g)}$, $CH_{(h)}$ of ferulic acid, respectively.

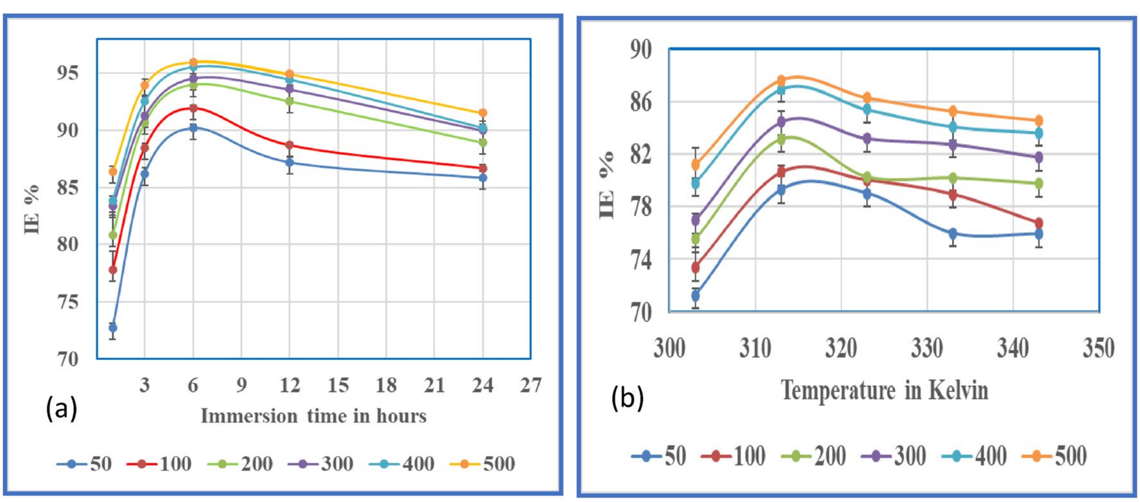

Fig. 4 Change in corrosion inhibition performance of FCS for mild steel in 1 M HCl at various **a** immersion periods, **b** temperatures

The remaining aromatic protons, namely $H_{(e–f)}$, show doublet signals at 7.1 ppm, 6.8 ppm, and 7.2 ppm. The proton signals at 5.2 ppm, 3.18 ppm, 3.7–4.5 ppm correspond to chitosan protons $H_{(1–6)}$ [43].

Comparative TGA and DSC curves of chitosan and FCS are shown in Fig. S1(a) and (b), respectively. TGA curve of chitosan reflects a weight loss of 50% at the degradation temperature range of 295–370 °C, whereas that of the modified polymer is 209–302 °C. The thermal stability of FCS is reduced compared to chitosan biopolymer. The decrease may be accounted due to the loose packing structure or reduction in the intermolecular hydrogen bonding [78, 81]. DSC curve of chitosan shows a broad endothermic peak at 122 °C that corresponds to the loss of moisture content bound to the polymeric backbone. The exothermic peak at 337 °C is attributed to the decomposition of chitosan. In contrast, the endothermic and exothermic peaks of FCS are found at lower temperatures than chitosan, i.e., at 114 °C and 210 °C, respectively [43].

Figure S2(a) and (b) reveals the zeta potential value and the average particle diameter distribution of FCS are + 49.5 mV and 383.3 nm, respectively. Polymers with a zeta potential value greater than 30 mV can show a more stable dispersion as the particles repel each other [82, 83]. Corrosion inhibitors with a positive zeta potential value can enhance corrosion protection. The positive surface charge on the inhibitor thus serves in adhering to the oxidized metal surface through the anions of the acid solution [84].

3.2 Measurement of the Anticorrosive Performance of FCS

3.2.1 Gravimetric Studies

Figure 4a portrays the change in the inhibition efficiency of FCS with varying immersion periods at 303 K. FCS showed the highest value of 95.96% when the metal samples were immersed in 500 ppm concentration of inhibitor solution. Such good anticorrosion performance can be corroborated with enhanced adsorption of the heteroatoms of the inhibitor on the metal surface [85]. Figure 4b displays the variation in the corrosion inhibition efficiency of FCS with the change in temperature from 303 to 343 K. The inhibition potential increases with temperature up to 313 K and after that is found to decrease slowly. Prolonged exposure of the metal surface to the inhibitor solution (> 6 h) and an increase in temperature (> 313 K) showed a slight decrease in the inhibition performance of FCS. The decreased stability of the adsorbed inhibitor on the longer exposure time and increased metal surface kinetic energy at higher temperatures may have led to the desorption process and hence a fall in efficiency [6, 86].

The corrosion rate and the temperature can be related by the Arrhenius and transition state equations represented by the Eqs. 6 and 7.

$$logK_{CR} = \frac{-E_a}{2.303RT} + \log A \quad (6)$$

$$log\frac{K_{CR}}{T} = \frac{R}{Nh}\exp^{\frac{\Delta S^*}{R}}\exp^{\frac{-\Delta H^*}{RT}} \quad (7)$$

where E_a is the apparent activation energy, ΔS^* and ΔH^* refers to the entropy and enthalpy of activation. Table 1 lists the activation parameters calculated from the linear plots drawn based on Eqs. 6 and 7, namely log K_{CR} vs. $1/T$ and log $(K_{CR/T})$ vs. $1/T$. The E_a values of the inhibited solutions are found to be less than that of the uninhibited solution. Such lower or unchanged E_a values can be corroborated with the chemical interaction between the metal and the heteroatoms of the FCS molecules [87, 88]. The increased inhibition

Table 1 Activation parameters for mild steel in acid solution without and with FCS

Conc. ppm	E_a kJ/mol	$A \times 10^{14}$ s^{-1}	ΔH^* kJ/mol	ΔS^* J/K
Blank	62.92	1.52	60.24	17.64
50	60.94	0.17	58.26	−0.53
100	61.09	0.17	58.41	−0.66
200	60.85	0.14	58.17	−2.12
300	59.53	0.07	56.85	−7.12
400	60.76	0.11	58.09	−4.35
500	60.79	0.10	58.11	−4.81

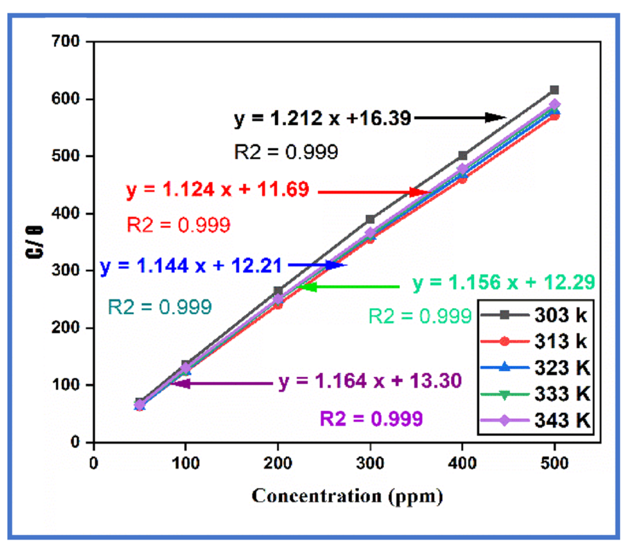

Fig. 5 Langmuir isotherm plot for mild steel in 1 M HCl without and with FCS

Table 2 Adsorption parameters for mild steel in 1 M HCl without and with FCS inhibitor at different temperatures

Temp K	K_{ads} L/mg	$-\Delta G_{ads}$ kJ/mol	ΔH_{ads} kJ/mol	ΔS_{ads} J/K	K_L
303	0.074	28.3	−2.888	0.022	0.083
313	0.096	29.9			0.066
323	0.093	30.8			0.067
333	0.094	31.7			0.067
343	0.087	32.5			0.072

performance of FCS with the temperature rise implies that chemisorbed passive film formation is higher than the dissolution rate. The lowering values of the frequency factor A can be correlated with the decreased corrosion rate in the presence of FCS [89]. The positive values of ΔH^* reveals that the metal dissolution involves an endothermic process. The negative values of ΔS^* declare the decrease in the disorderliness that may be due to the formation of the more orderly activation complex [90].

The inhibition efficiency relies on the corrosion inhibitor's quickness to diffuse from the solution to the metal surface. Thereby, it replaces the adsorbed water molecules and effectively binds to the active sites present on the surface [91]. The degree of surface coverage θ decides the nature and the mode of inhibitor adsorption [92]. The θ values at different temperatures were calculated using Eq. 8 and were fitted into various adsorption isotherm models. Based on the linear regression coefficient R^2 values, Langmuir adsorption isotherm represented by Eq. 9 was found to be the best fit.

$$\text{Surface coverage}\,\theta = \frac{W_b - W_i}{W_b} \tag{8}$$

$$\frac{C}{\theta} = \frac{1}{K_{ads}} + C \tag{9}$$

where C represents the inhibitor concentration, and K_{ads} refers to the equilibrium constant. Figure 5 displays the Langmuir plot, and slope values are found to deviate from unity. The deviation can be attributed due to the mutual attractive or repulsive interaction between the polar atoms or groups present in the polymers when adsorbed on the metal surface. On the contrary, the Langmuir isotherm equation was derived ignoring these interaction between the adsorbed molecules. In addition, the changes in the adsorption heat with increase in the surface coverage of the inhibitor was not included during the derivation of the Langmuir isotherm [93]. The slope deviation reveals that in addition to R^2 values, another physical characteristic K_L of the adsorption isotherm is to be considered for the best fit [94, 95]. K_L is referred to as the dimensionless separation factor of inhibitor adsorption and is related to K_{ads} by the following equation

$$K_L = 1/1 + K_{ads}C \tag{10}$$

The average values of K_L values calculated based on Eq. 6 is displayed in Table 2. According to Eduok and Khaled, if $K_L < 1$, then the adsorption process is considered favorable. If $K_L > 1$ or $K_L = 1$ then, the adsorption process is unfavorable or deemed to be irreversible [95]. Based on this literature, it is clear that the FCS inhibitor favors the Langmuir adsorption process.

Table 2 lists the other adsorption parameters calculated for mild steel in 1 M hydrochloric acid without and with FCS inhibitor. The standard free energy of adsorption ΔGads is calculated using the following equation:

$$\Delta G_{ads} = -RT\ln(1 \times 10^6 K_{ads}) \tag{11}$$

where R represents the ideal gas constant, T is the temperature in Kelvin, and 10^6 is the value of water concentration in ppm [96]. The negative values of ΔG_{ads} support the spontaneity of the adsorption process. When the values of ΔG_{ads} is less than 20 kJ/mole corresponds to physisorption, and greater than 40 kJ/mole conforms to chemisorption [97]. The ΔG_{ads} values listed in Table 2 lies between 28 and 32 kJ/mol. These values can be corroborated with the initial electrostatic interaction between the FCS inhibitor and the metal surface, leading to physisorption. The transfer of electron pairs from the heteroatoms to the empty d orbitals of Fe^{2+} ions and retro donation to the unoccupied π^* orbital of the FCS molecule occurs, resulting in the chemisorption process [98]. The value of K_{ads} also reflects the increased binding of the inhibitor molecules on the metal surface [21, 94].

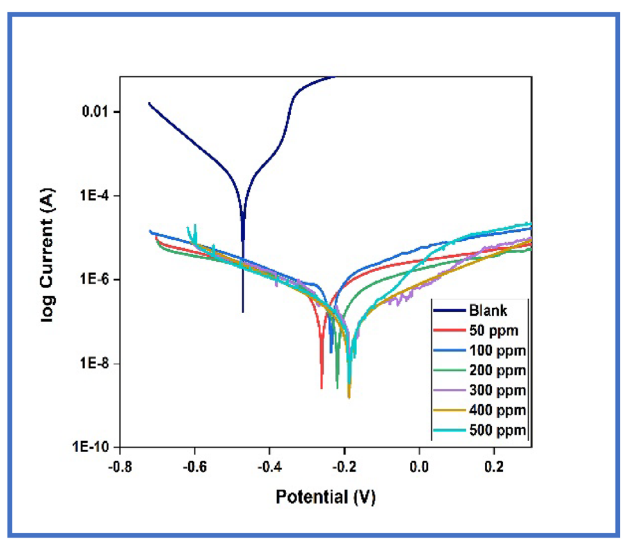

Fig. 6 Tafel plot for mild steel in 1 M HCl with and without FCS

Table 3 Tafel electrochemical parameters for mild steel in 1 M HCl without and with FCS

Conc. ppm	$-E_{corr}$ mV vs. SCE	$-\beta c$ mV/dec	βa mV/dec	$i_{corr} \times 10^{-3}$ µA/cm^2	IE %	LPR Ω cm^2	IE %
Blank	443	200.9	167	845		35.4	
50	241	169.7	291.8	143.4	83.0	222.1	84.1
100	257	137.4	276.3	125.3	85.2	294.4	87.9
200	244	141.4	123.7	110.3	87.0	365.7	90.3
300	219	157.7	174.3	68.9	91.9	488.8	92.7
400	187	125.4	128.3	23.3	97.2	754.5	95.3
500	189	123.8	115.6	22.4	97.4	797.4	95.6

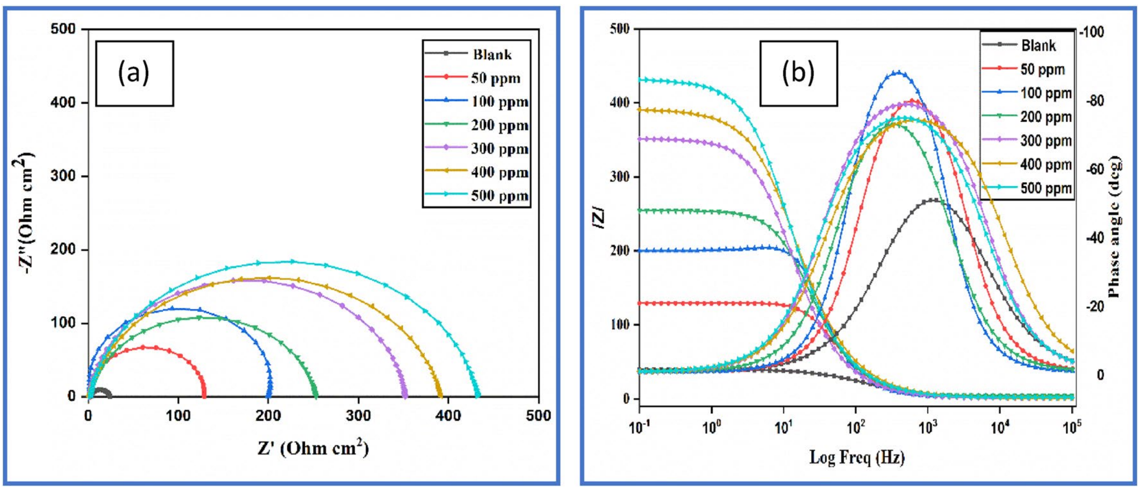

Fig. 7 **a** Nyquist spectra, **b** impedance bode modulus plots for mild steel in 1 M HCl without and with FCS inhibitor at 303 K

3.2.2 Electrochemical Measurement Techniques

3.2.2.1 Polarization/Tafel Studies Tafel studies help to analyze the influence of the inhibitor to mitigate the corrosion process taking place at the anode or cathode or both. Figure 6 illustrates the polarization curves obtained for mild steel at room temperature in the absence and presence of FCS inhibitor. The Tafel plot depicts the decrease of current density with an increase in FCS concentration. The decrease implies that the inhibitor film formed impedes the passage of aggressive ions to the metal surface [95]. Table 3 display the various corrosion parameters obtained from the Tafel polarization curves. The E_{corr} values can be related to the driving force towards the corrosion reaction. Higher E_{corr} values imply a greater energy requirement for the corrosion reaction to take place [99]. The positive shift of E_{corr} values from −443 to −189 mV illustrates the corrosion inhibition performance of the inhibitor [100]. This potential shift is further supported by the lowering of the corrosion current i_{corr} density [30]. The change in both anodic (βa) and cathodic Tafel slopes (βc) reveals that the inhibitor influences both cathodic and anodic reactions but predominantly anodic [101]. The LPR values increases with the concentration of the FCS polymer as displayed in Table 2. This increase indicates a decreased metal dissolution due to the adsorption of the inhibitor molecules on the metal surface. The inhibition efficiency calculated using i_{corr} values showed a maximum of 97.4% for 500 ppm concentration which matches with those calculated from LPR values.

3.2.2.2 AC Electrochemical Impedance Studies EIS technique has emerged out as an excellent tool to study the effectiveness of the corrosion inhibitors, both qualitatively and quantitatively [102]. Figure 7a and b represents the Nyquist and Bode plots obtained for mild steel in blank and in the presence of FCS. The Nyquist plot clearly shows an increase in the diameter of the impedance plot with the inhibitor concentration. This increase can be attributed to the inhibitor film formation by protecting the metal surface from corrosion [103]. The inhibition of corrosion is further supported by the rise in the phase angle with the increase in the inhibitor's concentration, as shown in the Bode plot [104]. The Bode plot reveals only one time constant, which can be corroborated with the corrosion inhibition by the charge trans-

Table 4 EIS parameters for mild steel in 1 M HCl without and with FCS

Conc	$\chi^2 \times 10^{-3}$	R_s	CPE		$C_{dl} \times 10^{-5}$	R_P	IE
			n	$Y_o \times 10^{-6}$			
ppm		Ω cm^2		Ω^{-1} S^n cm^{-2}	µF/cm^2	Ω cm^2	%
Blank	0.081	2.085	0.879	316.2	10.592	21.7	
50	2.541	2.998	0.884	135.4	7.943	126.9	82.9
100	1.223	3.085	0.933	92.7	6.953	196.7	88.9
200	1.554	3.085	0.911	55.4	3.648	250.4	91.3
300	2.332	1.008	0.884	41.9	2.408	350.7	93.8
400	2.995	1.558	0.962	33.7	2.840	390.7	94.5
500	1.685	1.685	0.874	30.6	1.639	430.7	94.9

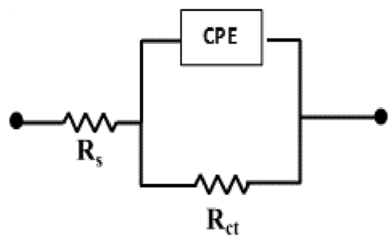

Fig. 8 Equivalent circuit

fer process and is not changed by the inhibitor's presence [105]. The semi-circle in the Nyquist plot is not perfect due to the metal surface's inhomogeneity, surface irregularities, impurities, surface active sites collectively referred as frequency dispersion effect [98, 106]. Hence the capacitor in the equivalent circuit is replaced by the constant phase element to compensate the depression in the semi-circle [107]. Table 4 lists the equivalent circuit fitted impedance parameters, and Fig. 8 displays the equivalent circuit. The double-

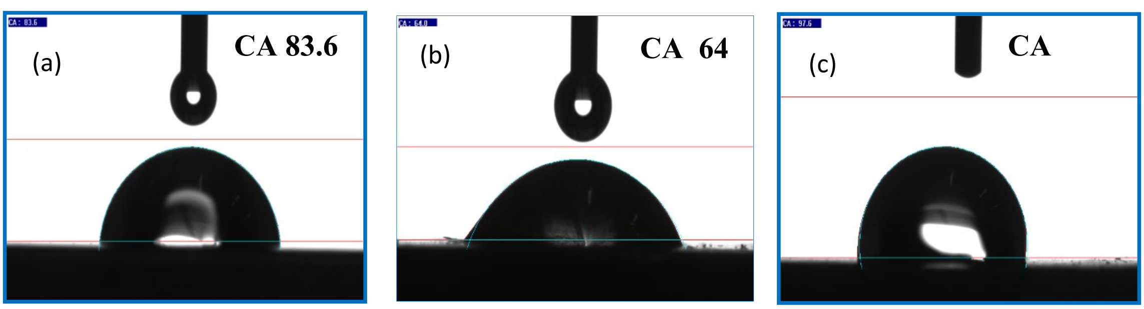

Fig. 9 Contact angle of mild steel surfaces **a** plain, **b** exposed to acid, **c** exposed to acid containing the FCS inhibitor

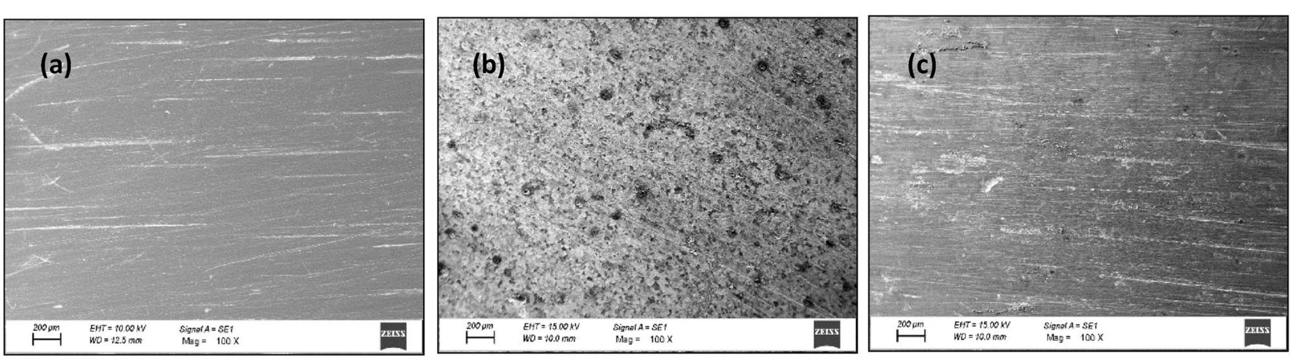

Fig. 10 SEM image of the mild steel surfaces **a** plain, **b** exposed to acid, **c** exposed to acid containing FCS

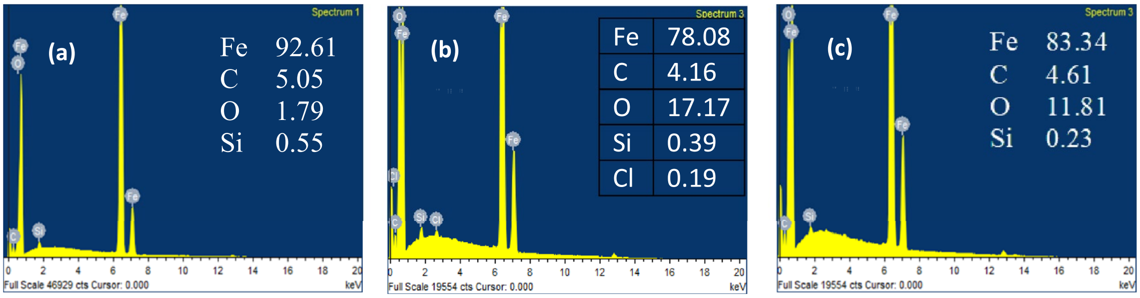

Fig. 11 EDAX image of surfaces **a** plain metal, **b** exposed to 1 M HCl, **c** exposed to 1 M HCl containing FCS

layer capacitance C_{dl} can be calculated from the magnitude of constant phase element Y_0 values using the Eq. 12.

$$C_{dl} = \left(Y_0 * R_{ct}{}^{1-n}\right)^{1/n} \quad (12)$$

The decreasing C_{dl} values and increasing charge transfer resistance (R_p) values ith FCS concentration can be correlated with the increased thickness of the protective film leading to an increased corrosion inhibition [108].

3.3 Surface Characterization

3.3.1 Contact Angle Measurements

Figure 9 displays the contact angle of (a) plain metal surface, (b) & (c) the metal surfaces exposed to acid and acid containing FCS, respectively. An angle of 90° or less indicates that the steel surface is hydrophilic and higher than 90° hydrophobic. The enhanced hydrophobic nature of the inhibitor immersed metal sample reveals the FCS's adsorption on the metal surface, leading to the protective film formation [109–111].

3.3.2 Field Emission Scanning Electron Microscopic Analysis

Figure 10a portrays the scanning electron microscopic images of the metal surface before exposure to the acid solution. Figure 10b depicts the extensive damage produced when the metal sample is in contact with the aggressive acid medium in the inhibitor's absence. Figure 10c reflects the resistance offered by the FCS inhibitor against the metal dissolution as the surface is smooth as that of the plain metal.

3.3.3 Energy Dispersive X-ray Analysis

EDAX images with % of different element contents of the bare metal surface, surface exposed to uninhibited and inhibited acid solution are displayed in Fig. 11a–c.

The rich iron content peak in Fig. 11a portrays the polished mild steel surface [62]. The surface damage of the metal surface and the reduction in the corrosion active sites when immersed in the absence and presence of FCS containing acid solution can be explained by comparing Fig. 11b and c, respectively. The presence of oxygen and chlorine peaks in Fig. 11b reflects the formation of the corrosion products such as chlorides and oxides on the mild steel surface [112, 113]. On the other hand, suppression in the oxygen and chlorine peaks, increase in iron and carbon content supports the formation of the organic polymer film on the surface inhibiting the corrosion [114, 115].

3.3.4 Optical Profilometric Studies

Figure 12a–c portrays the optical profilometric images of the bare metal surface and surfaces exposed to uninhibited and inhibited solution. Arithmetic average roughness value (Sa) and the root mean square roughness value (Sq) for the well-polished plain metal surface were found to be 1.551 µm and 1.977 µm, respectively. The metal surface exposed to uninhibited acid solution showed an increased roughness value of 3.371 µm (Sa) and 4.456 µm (Sq). However, the metal surface exposed to an acid solution containing an optimum FCS concentration has shown a decreased surface roughness value of 1.597 µm (Sa) and 2.305 µm (Sq). This decrease may be corroborated with the reduction in corrosion in the presence of the inhibitor [116].

3.3.5 Atomic Force Microscopy (AFM)

AFM is a useful tool for monitoring the corrosion processes by visualizing the surface morphology of different materials. Figure 13 represent AFM (2 D and 3 D) images of the bare metal surface, metal surface exposed to uninhibited and inhibited solution, for 6 h. It is evident from Table 5 that the average roughness value and root mean square value of the metal sample exposed to acid containing FCS shows a

Fig. 12 3D images of mild steel surfaces **a** plain metal, **b** exposed to acid and **c** exposed to acid containing FCS

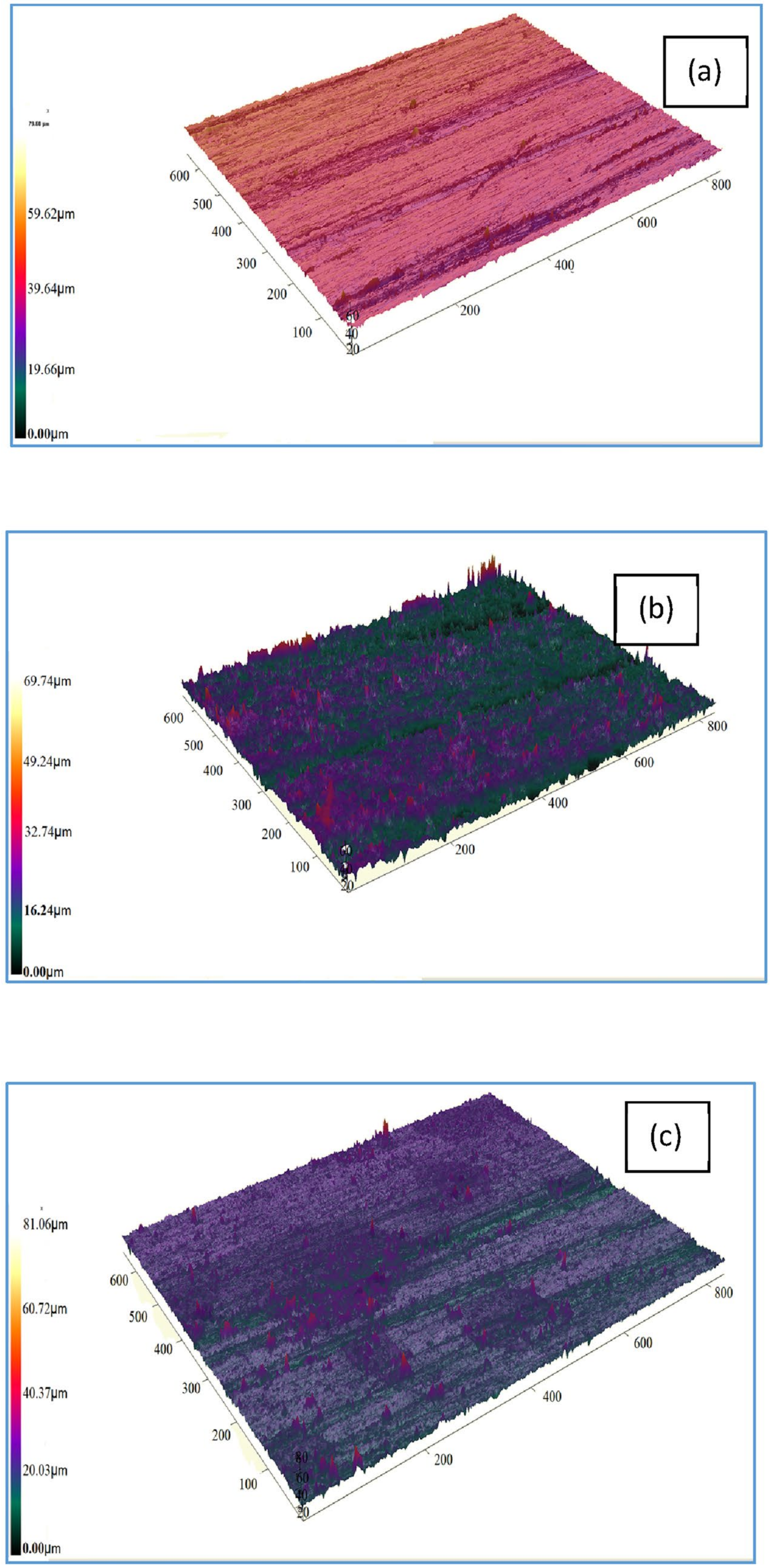

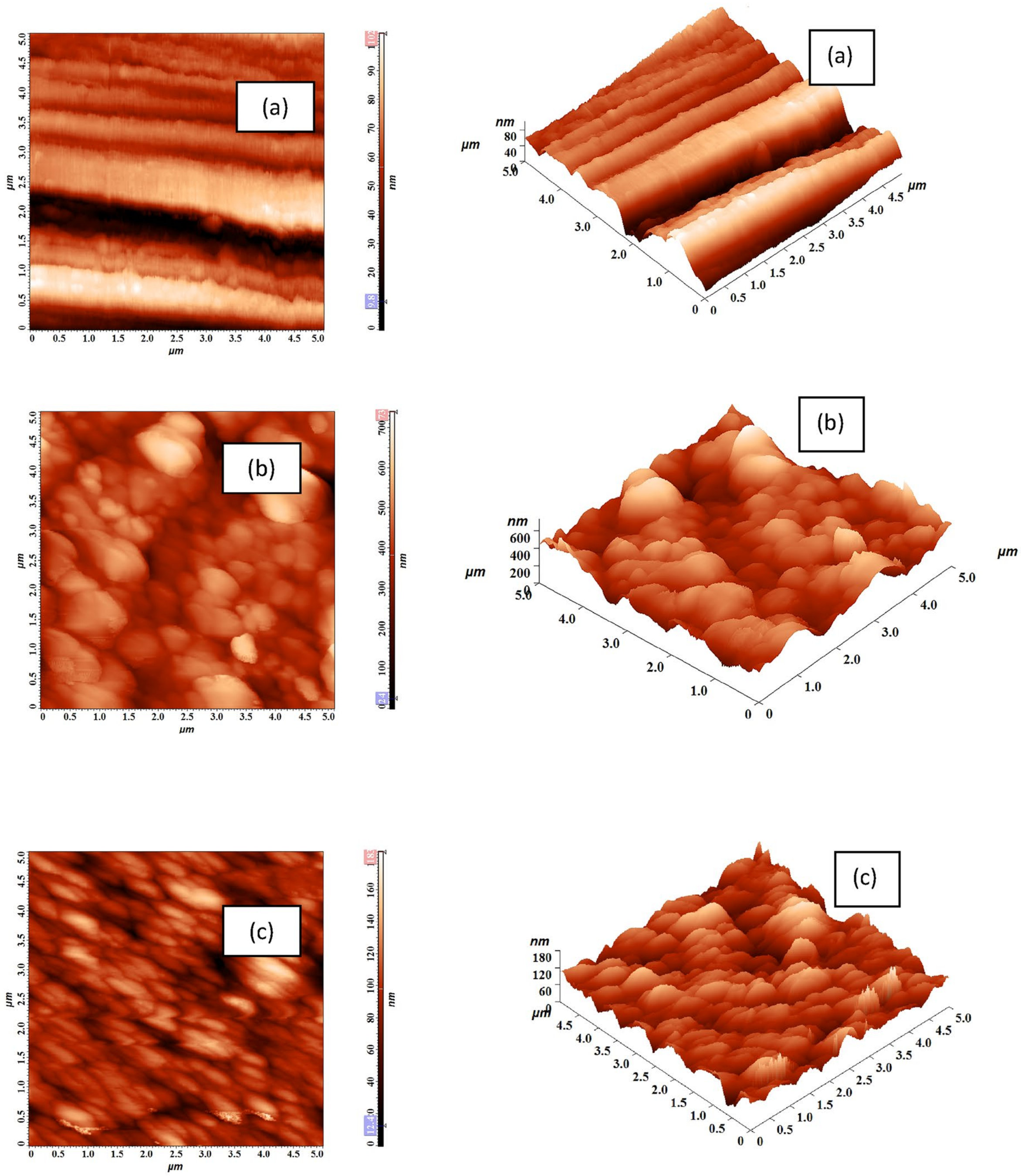

Fig. 13 AFM image of surfaces **a** plain metal, **b** exposed to 1 M HCl and **c** exposed to 1 M HCl containing FCS

Table 5 AFM parameters for mild steel surface exposed to acid without and with FCS

Samples	Average roughness Sa (nm)	Root mean square Sq (nm)	Peak to peak height (nm)
Plain metal	14.45	19.12	102.88
Surface exposed to 1 M HCl	66.94	84.83	739.41
Surface exposed to 1 M HCl + FCS	17.07	21.80	183.50

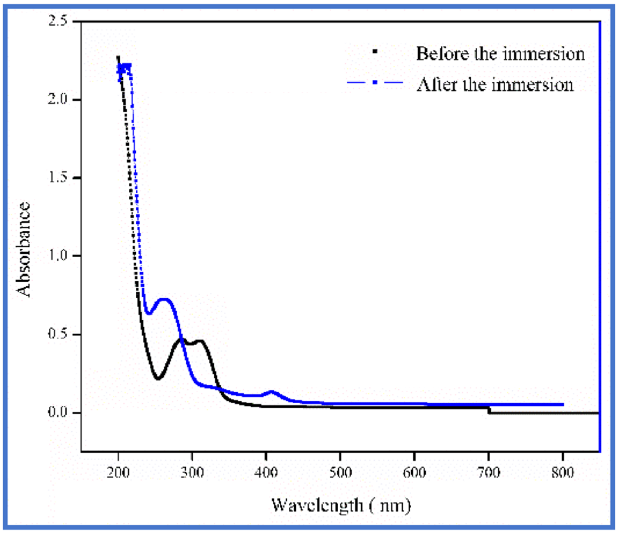

Fig. 14 UV–visible spectra of FCS solution before and after introducing the mild steel samples

significant decrease. This result can be corroborated with the film formed by the inhibitor adsorbed on the metal surface [117].

3.3.6 UV Spectral Analysis

Figure 14 depicts the UV–visible spectra of FCS solution before and after the immersion of mild steel samples. The UV–vis spectrum of FCS solution before immersion of the metal samples show absorption bands at 290 nm and 321 nm. These bands correspond to the π–π* electronic transitions of the aromatic ring and n–π* transitions by the lone pair of electrons on the nitrogen and carbonyl group, respectively [118]. On the other hand, the UV–vis spectrum of the FCS solution taken after 6 h of immersion of metal samples shows an increase in the absorbance bands from 321 to 266 nm (blue shift). Besides, the absorbance band at 290 nm is disappeared. The increase and change in the position of the absorbance band can be corroborated with the strong interactions of the heteroatoms of the FCS inhibitor and the Fe^{2+} ions resulting in the complex formation [119–122].

4 Theoretical Studies

4.1 DFT Studies

DFT studies serve as a successful tool in predicting the reciprocity between the inhibitor and the metal. The theory throws light on the chemical reactivity and selectivity of corrosion inhibitors, thereby aid to propose a suitable mechanism for the corrosion inhibition process. The quantum chemical calculations were performed for the neutral FCS molecule and also for the protonated form as the study is done in an acid medium. These calculations will enable identifying the preferred form of the inhibitor that can selectively interact with the metal surface.

Figure 15 displays the optimized geometry, frontier molecular orbitals, electrostatic potential mapping of the FCS in both neutral and protonated forms. The protonation site in the FCS molecule was decided based on the proton affinity values calculated using the following equation

$$PA = E_{\text{prot}} + E_{\text{water}} - E_{\text{non}_{\text{prot}}} - E_{\text{hydronium ion}}$$

where, the term are the corresponding sum of electronic and thermal enthalpies of the protonated inhibitor, neutral inhibitor, water and hydronium ion [123, 124]. The protonation of FCS as supported from DFT calculations (results presented in Table 6) involves the amino group of the molecule.

The electron density distribution plots of the frontier molecular orbitals, i.e., HOMO and LUMO orbitals, are useful to locate the preferred sites of adsorption in the inhibitor molecules. The electron distribution is solely on the ferulic acid moiety and the methyl group of the methoxy group of the ferulic acid moiety is found to contribute to a smaller extent to the HOMO and no contribution to the LUMO; in both neutral and protonated forms. This suggests the charge transfer by the –CH_3 group of ferulic acid through s—type HOMO and the heteroatoms of the chitosan moiety to the vacant orbital d orbital of the Fe on the mild steel surface [125]. The electrostatic potential structure reveals the nucleophilic region (red color) and the electrophilic region (blue) of the FCS inhibitor [126].

Table 7 gives quantum chemical parameters calculated based on the density functional theory for the neutral and protonated FCS molecule. The E_{HOMO} and E_{LUMO} values provide valuable information regarding the electron donating and accepting capacity of the neutral and protonated FCS molecule. The greater the value of E_{HOMO}, the more it behaves as an electron donor, and the lower E_{LUMO} value characterizes electron acceptors. When an inhibitor shows a tendency to donate electrons to the metal surface and at the same time tends to accept the electrons back donated by the metal, then stronger is the adsorption process [29, 127]. Table 6 reveals that neutral and protonated molecules behave as an electron donor and a good electron acceptor, respectively. This behavior can be corroborated with the increased global electronegativity (χ), electrophilicity index (ω) values of the protonated FCS molecule, and the higher fraction of the electron transfer (ΔN) value for the neutral molecule [29]. Electrophilicity index value denotes the energy stabilization after accepting the additional electrons from the environment. The energy gap (ΔE) between the frontier molecular orbitals measures the kinetic stability of the corrosion inhibitor [128]. Smaller energy gap values indicate lesser kinetic stability and hence greater reactivity with the metal surface. Thus, protonated form contributes to the better performance of the inhibitor than that of the neutral molecule. Dipole moment (μ) values can be related to the electrostatic interaction between the inhibitor molecules and the metal surface. The higher values of the dipole moment reveal that protonated molecule contributes physisorption process compared to that of the neutral molecule [129].

4.2 Monte Carlo and Molecular Dynamic Simulation Studies

The interaction of the FCS and FCS-H+ onto the Fe (110) surface offers a mean to calculate the adsorption energetics of this adsorption process. Quantitatively, this is done by

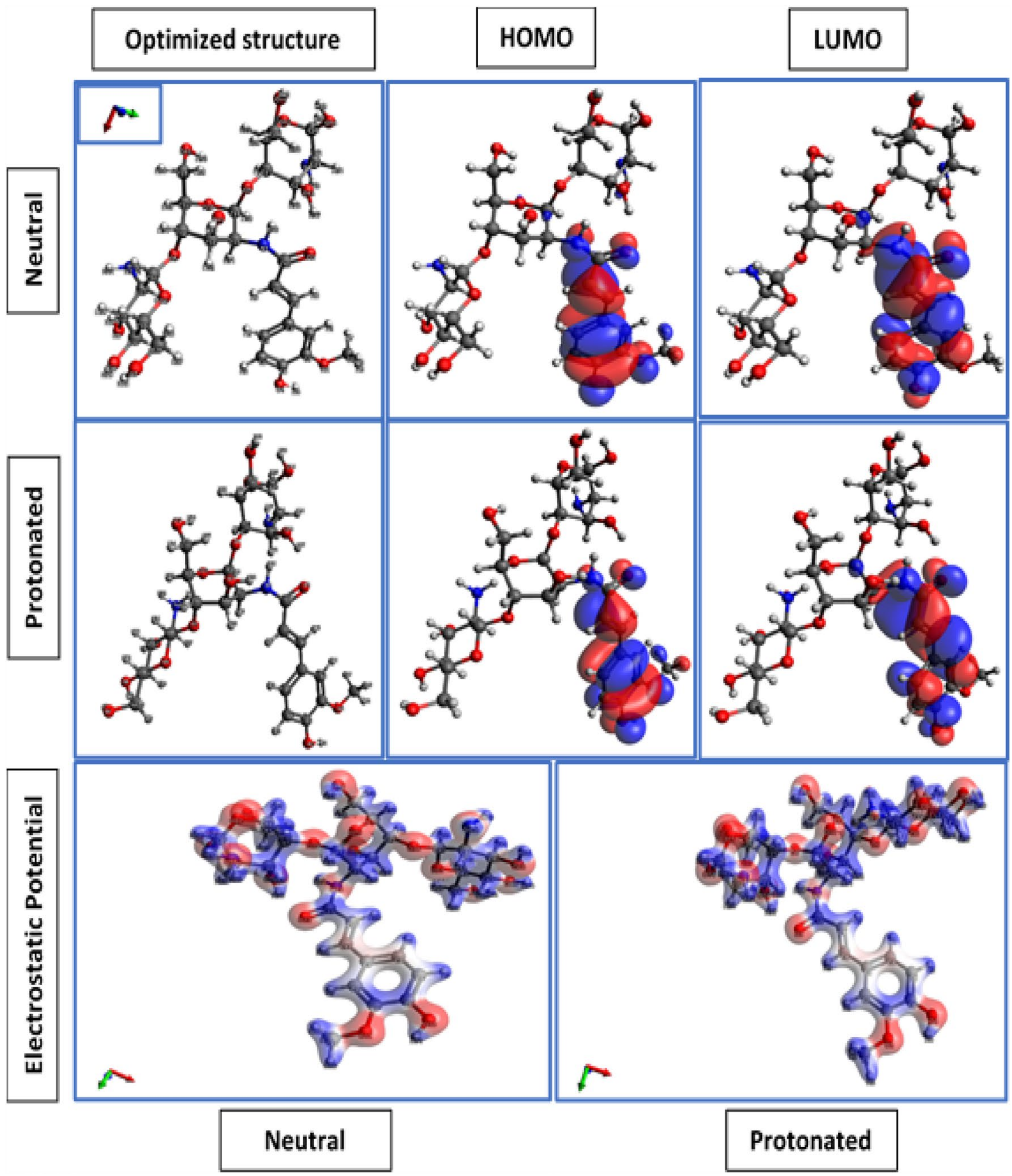

Fig. 15 Optimized molecular structure, frontier MO and electrostatic potential mapping of neutral and protonated FCS

Table 6 Sum of electronic and thermal enthalpies (SE & TE) and the calculated proton affinity (PA) for the inhibitor

Molecule	SE & TE	PA
FCS	− 2460.525645	
$FCS\text{-}H^+$	− 2460.917701	− 0.12273
H_2O	− 76.422344	
H_3O^+	− 76.691667	

Table 7 Quantum chemical parameters of neutral and protonated FCS molecule

Parameters	Neutral	Protonated
E_{HOMO} (eV)	− 3.5991	− 4.6901
E_{LUMO} (eV)	− 1.1506	− 2.4206
Band gap (eV)	2.4483	2.2690
Ionisation potential (I.P)	3.5991	4.6901
Electron affinity (EA)	1.1506	2.4206
Electronegativity (χ)	2.3749	3.5554
Global hardness (η)	1.2243	1.1348
Global softness (σ)	0.8168	0.8812
Electrophilicity index (ω)	1.1517	2.7849
Δ*N*	0.9986	0.5572
Dipole moment	8.4876	13.7347

calculating the adsorption energy (E_{ads}) using the following equation [31, 69, 75, 130–136]:

$$E_{adsorption} = E_{Fe\ (110)_{||}FCS\ or\ FCS\text{-}H+} - \left(E_{Fe\ (110)} + E_{FCS\ or\ FCS\text{-}H+}\right) \quad (13)$$

where $E_{Fe(110)_{||}FCS\ or\ FCS-H+}$ is the total energy of the simulated corrosion system, $E_{Fe,}$ and $E_{FCS\ or\ FCS-H+}$ are the total energy values of the Fe (110) surface and the free inhibitor molecules (in their neutral or protonated state) [31].

The lowest energy configuration of FCS and FCS-H+ on the Fe (110) surface is presented in Fig. 16. The inhibitor is absorbed on the Fe (110) surface in a geometry that takes advantage of the surface contact through its oxygen atoms.

The energy values (in terms of different contributions) over the random MC configuration search are shown in Fig. 17. After 3,000,000 MC steps as perceived from the graph, the value of total average energy is equilibrated, indicating that the lowest energy configuration of the inhibitors was attained.

The Eads. distribution of the FCS and FCS-H+ inhibitor gained by a massive number of unsystematic configurations from Monte Carlo calculations (values of adsorption energies for ten lowest energy poses are presented in supporting information Table S1) is presented in Fig. 18.

The corrosion inhibitor mitigate corrosion by adsorbing on the metal surface replacing the water molecules. The negative values obtained for the adsorption energy of the FCS inhibitor, water molecules and the aggressive species namely H_3O^+ and Cl^- ions on Fe (110) surface indicates the spontaneity of the adsorption process. Also, the greater adsorption energy values obtained for the FCS inhibitor compared to water, H_3O^+ and Cl^- ions reveals the adsorption strength of the FCS inhibitor on the Fe (110) surface. This remarkable ability of FCS makes it a significant corrosion inhibitor for iron surface in HCl solution [137, 138]. The E_{ads} onto Fe surface values (Fig. 18) for the FCS adsorption is from − 239.35 to − 285.55 kcal/mol (with the maximum value of Eads probability distribution at –262.15 kcal/mol). The adsorption energies are higher for the protonated form of the FCS molecule (namely FCS-H+). They are in the range of − 372.95 to − 415.86 kcal/mol (with the maximum value of Eads probability distribution at − 395.85 kcal/mol). These huge Eads. are suggestive of a strong adsorptive interaction of this inhibitor with the Fe (110) surface [67, 68, 132].

MD poses presented in Fig. 19, show that the adsorption of these molecules, although in its neutral state, only covers a small fraction of the iron surface. In the case of the protonated FCS it's adsorption properties increase—in this case, the molecule tends to have a flat geometry onto the Fe (110) surface (the equilibration of the temperature and the energy terms during the MD simulations are shown in the supporting information).

A modest method to attain the information vis-à-vis the adsorption process is to use the RDF peak appearance distance [68, 70, 75, 131, 139]. The peak presence for the FCS and FCS-H+ inhibitor is at a lesser distance than 3.5 Å from the surface of Fe indicates the chemisorption process, while for physisorption, this is projected at larger distances. As evidenced in Fig. 20, the RDF value for nitrogen and oxygen atoms in the FCS-H+ case is present at 3.01 Å (O) and 3.07 Å (N) from the Fe (110) surface—an expected value for the chemisorption process. Whereas for the FCS, accountable atoms for the absorption are oxygen atoms [RDF is 2.97 Å (O)]; the nitrogen atoms, as evidenced from the RDF distance of 8.80 Å (N) are do not contribute to the adsorption process. The corresponding RDF analysis support that the chemisorption is involved during the adsorption of the inhibitor that decreases the corrosion rate of the Fe (110) surface [66, 67, 69, 71, 130, 140].

4.2.1 Corrosion Inhibition Mechanism

Corrosion inhibitors adopt surface-based adsorption mechanism to protect the metal from corroding when exposed to aggressive environment.The inhibitor molecules get adsorbed on the metal surface replacing the already adsorbed

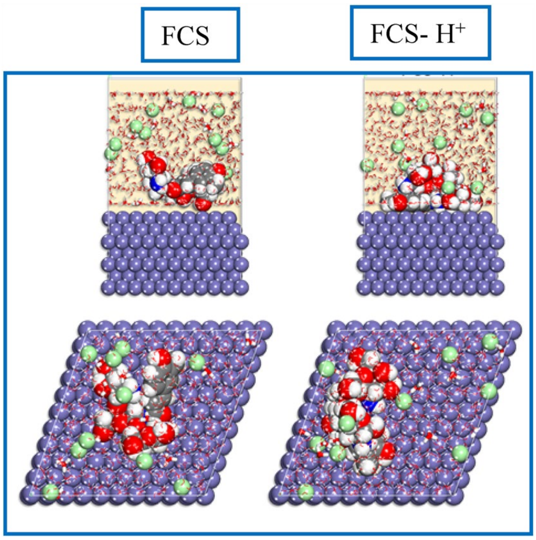

Fig. 16 MC poses the lowest adsorption configurations for the FCS and FCS-H+ in the simulated corrosion media on the Fe (110) surface

water molecules [141]. The adsorption mechanism include both physisorption, chemisorption and electrostatic adsorption. Physisorption involve a weak Vander waals force of attraction and that the adsorbed inhibitor on the metal surface may be easily desorbed with raise in temperature. On the other hand, chemisorption involve the formation of covalent bonds due to the exchange of electrons between the surface sites of the metal and the inhibitor molecules. While, electrostatic adsorption involves coloumbic force of attraction between charged metal surface and the charged functional groups. Based on the corrosive medium employed and nature of the polymer used, corrosion inhibitor adsorption can occur via physisorption, chemisorption, electrostatic adsorption or all the three modes of adsorption.The present study involves acid medium, so preferentially electrostatic adsorption come into play as FCS is in protonated form. On the other hand the anions of the acid medium namely Cl^- adsorbed on the oxidised metal surface literally attracts the protonated FCS towards it. This aid in the surface coverage of the inhibitor which increases with the increase in inhibitor concentration. The electrostatically attracted protonated FCS may now interact chemically with the metal surface leading to chemisorption. The chemisorption process encountered in the inhibition study is supported by the increase in inhibition with increase in temperature and also from Ea values. Further support comes from the lower energy gap values of the protonated FCS compared to neutral FCS by DFT study. The Monte Carlo and molecular dynamics simulation studies and RDF analysis further endorse the preferential adsorption of the protonated FCS on the metal surface through chemisorption process. Though the dipole moment value indicates a physisorption process, a large molecule like FCS can show numerous such weak vanderwaals forces leading to summative interactions stronger like chemisorptions [142]. Hence, in case of large molecules a mixed adsorption process is encountered. The presence of the lone pair of electrons on the functional groups present in the polymer can act as a ligand forming metal ligand complexes as was reflected in the UV spectral studies.

4.2.2 Comparative Study of Corrosion Inhibition Efficiency

The inhibition efficiency of the FCS corrosion inhibitor evaluated in the present study is compared with that of chitosan and ferulic acid from which it was prepared. The chitosan which is water insoluble showed a corrosion

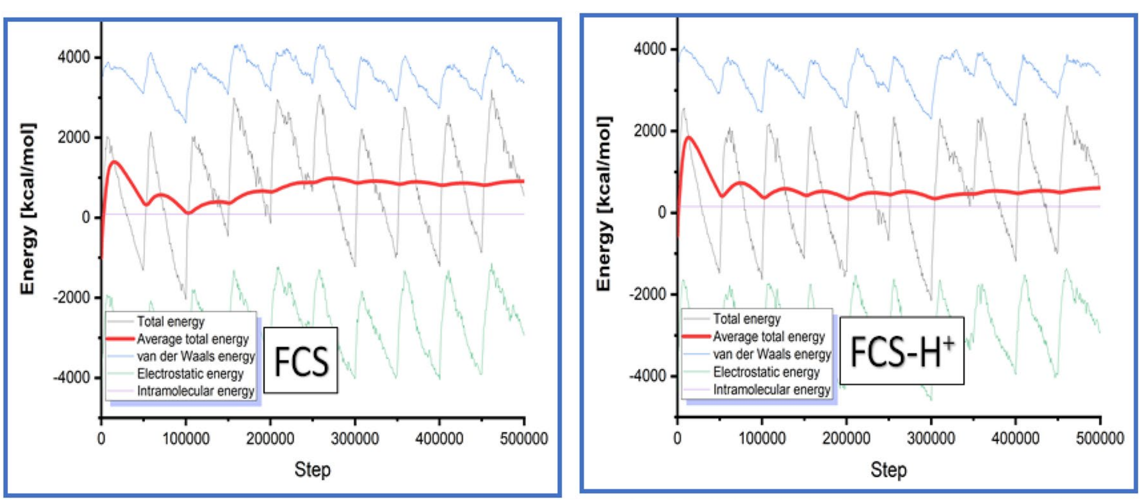

Fig. 17 The presentation of the different energy terms contributions during the Monte Carlo calculations for FCS (neutral) and FCS-H+ (protonated) inhibitor molecule

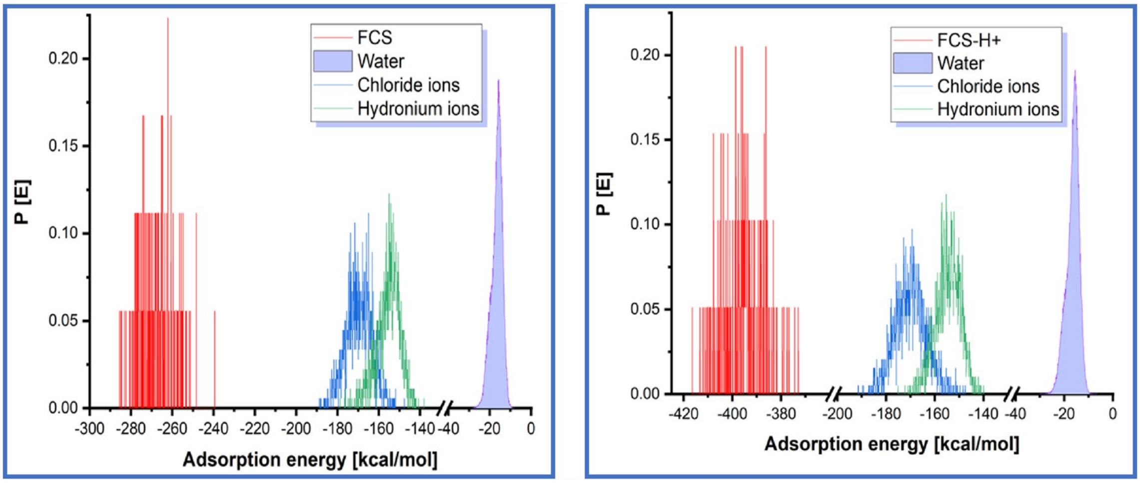

Fig. 18 Distribution of adsorption energies for: FCS (neutral) and FCS-H+ (protonated) inhibitor onto the Fe (110) surface

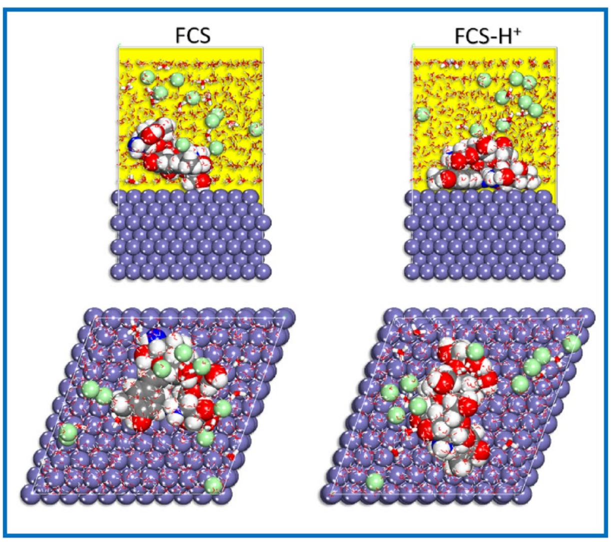

Fig. 19 MD poses the lowest adsorption configurations for the FCS and FCS-H+ in the simulated corrosion media on the Fe (110) surface

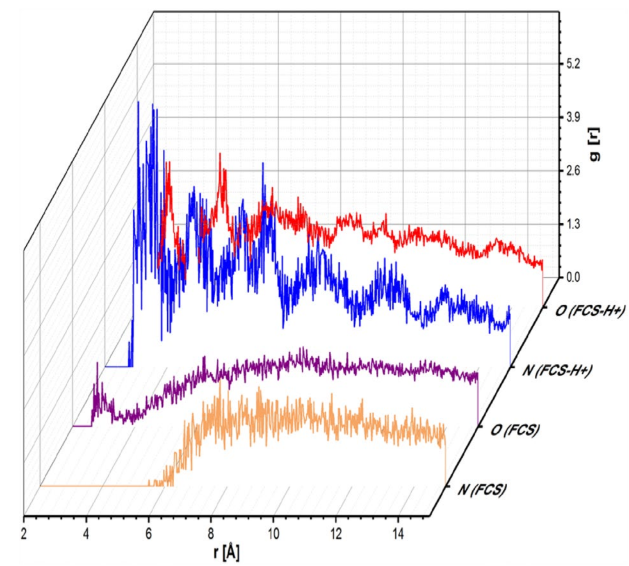

Fig. 20 RDF of heteroatoms (nitrogen and oxygen,) for FCS and FCS-H+ on the Fe surface obtained from MD trajectory

inhibition efficiency of 96% at 60 °C by weight loss studies while the Tafel and Impedance studies record of 68% and 61.5%, respectively, for mild steel in 0.1 M HCl solution [143]. Rabizadeh and Khameneh Asl reported corrosion inhibition efficiency of chitosan to be 92.1% for mild steel in 0.1 M HCl for an immersion period of 24 h at 298 K [144]. Neeraj et al. compared the corrosion inhibition efficiency of chitosan alone and in combination with KI for mild steel in 1M sulfamic acid and showed that an addition of 5 ppm KI to 200 ppm chitosan improved the inhibition efficiency from 73.8 to 90% [145]. Similarly Solomon et al. investigated the inhibition efficiency of chitosan which was found to be 46.98% and was almost doubled when incorporated with silver nanoparticles (94.98%) for St37 steel in 15% H_2SO_4 [146, 147]. Okoronkwo et al. evaluated the corrosion inhibition efficiency of chitosan extracted from snail shells and have reported an inhibition efficiency of 93.2% by weight loss studies for plain carbon steel (mild steel) in acid media [148]. Ferulic acid, a constituent of Kraft and Soda lignins extracted from oil palm empty fruit bunch extract and from spent ground coffee extract is accounted for good anticorrosive activity for mild/carbon steel in neutral solution and acid solution, respectively [149–151]. Biobased aromatic acids that include ferulic acid showed potential as additive for mild steel protection in immersion or partial immersion applications in water-based electrolytes [152]. The corrosion

Table 8 Comparison of the inhibition efficiency of FCS with other corrosion inhibitors for mild steel in HCl solution

Corrosion inhibitor	IE%	Inhibitor conc.	Ref.
I. Plant extracts			
Cryptocarya nigra barks	91.05%	500 ppm	[57]
Spilanthes acmella Leaves	93.04%	10% v/v	[155]
Eucalyptus leaf	90%	800 ppm	[156]
Ammi visnaga L. *Lam* seeds	84%	1 g/l	[157]
Rosa canina fruit	86%	800 ppm	[158]
II. Synthetic organic compounds			
2-Mercaptobenzimidazole derivatives	93%	5×10^{-3}	[159]
Triazole-based compounds	> 90%	850 µM	[160]
Coumarin derivative	96%	0.5 mM	[161]
13-Docosenoic acid amide derivatives	96.8%	500 ppm	[162]
Pyrazole carboxamide derivatives	84.56%	4×10^{-4} mol l^{-1}	[163]
III. Modified chitosan derivatives			
Sodium lauryl sulfate modified chitosan	94.66%	500 ppm	[31, 46]
Disodium EDTA functionalized chitosan	96.63%	500 ppm	[32]
8-Hydroxyquinoline based chitosan	93%	10 ppm	[75, 135]
Chitosan Schiff bases	91.74%	150	[164]
FCS	97.4%	500	Present study

inhibition potential of ferulic acid as active constituents in plant extracts such as *Juglans regia* for mild steel in 3.5 weight % NaCl solution and *Hemerocallis fulva* against aluminium in sulphuric acid solution were also studied [153, 154].

The inhibition efficiency comparison of FCS with the other corrosion inhibitors employed for mild steel in 1 M HCl solution is displayed in Table 8.

5 Conclusion

- The corrosion inhibition performance of FCS reached 95.96% at 500 ppm and 6 h of immersion period.
- Thermodynamic activation and adsorption parameters namely E_a and ΔG_{ads} endorse a mixed adsorption process involving an initial electrostatic interaction followed by chemisorption of the inhibitor molecules on the metal surface. This conclusion is further supported by the increase in the inhibition efficiency with increase in temperature.
- Tafel studies showed that the FCS inhibitor was a mixed type inhibiting both the cathodic hydrogen evolution and anodic dissolution of the mild steel metal.
- Protonated molecule contributes to the inhibitor efficiency more than that of the neutral molecule.
- FCS shows that it is an efficient, green corrosion inhibitor that can be used as an additive during acid cleaning of mild steel.
- MC and MD calculations validate that there is a vigorous adsorptive interaction that takes place amongst the FCS inhibitor (in the neutral and protonated state) and the Fe surface. The obtained theoretical results are in good agreement with the experimental results.

Supplementary Information The online version contains supplementary material available at https://doi.org/10.1007/s40735-023-00796-z.

Acknowledgements The authors would like to thank Indian Institute of Science, Bangalore, India for doing the computational analysis. Avni Berisha gratefully acknowledges the support from the Ministry of Education, Science and Technology of Kosovo (Nr.2-5069) for providing the computing resources.

Author Contributions SJHMJ: conceptualization, methodology, writing- original draft preparation. AB and VM: writing, computational software Monte Carlo simulation studies, SSS: electrochemical studies SS: supervision, reviewing and editing.

Funding The authors declare that they have no known competing financial interests or personal relationships that could have appeared to influence the work reported in this paper. No funding received.

Data Availability Supplementary materials attached.

Declarations

Conflict of interest On behalf of all authors, the corresponding author states that there is no conflict of interest.

Ethical Approval Not applicable.

References

1. Alamry KA, Aslam R, Khan A, Hussein MA, Tashkandi NY (2022) Evaluation of corrosion inhibition performance of thiazolidine-2,4-diones and its amino derivative: gravimetric, electrochemical, spectroscopic, and surface morphological studies. Process Saf Environ Prot 159:178–197
2. Sherif ESM (2014) The role of corrosion inhibitors in protecting metallic structures against corrosion in harsh environments. Elsevier, Amsterdam
3. Finšgar M, Jackson J (2014) Application of corrosion inhibitors for steels in acidic media for the oil and gas industry: a review. Corros Sci 86:17–41. https://doi.org/10.1016/j.corsci.2014.04.044
4. Mobin M, Rizvi M, Olasunkanmi LO, Ebenso EE (2017) Biopolymer from tragacanth gum as a green corrosion inhibitor for carbon steel in 1 M HCl solution. ACS Omega 2:3997–4008. https://doi.org/10.1021/acsomega.7b00436
5. Peter A, Obot IB, Sharma SK (2015) Use of natural gums as green corrosion inhibitors: an overview. Int J Ind Chem 6:153–164. https://doi.org/10.1007/s40090-015-0040-1
6. Fares MM, Maayta AK, Al-Qudah MM (2012) Pectin as promising green corrosion inhibitor of aluminum in hydrochloric acid solution. Corros Sci 60:112–117. https://doi.org/10.1016/j.corsci.2012.04.002
7. Fiori-Bimbi MV, Alvarez PE, Vaca H, Gervasi CA (2015) Corrosion inhibition of mild steel in HCL solution by pectin. Corros Sci 92:192–199. https://doi.org/10.1016/j.corsci.2014.12.002
8. Umoren SA, Obot IB, Madhankumar A, Gasem ZM (2015) Performance evaluation of pectin as ecofriendly corrosion inhibitor for X60 pipeline steel in acid medium: experimental and theoretical approaches. Carbohydr Polym 124:280–291. https://doi.org/10.1016/j.carbpol.2015.02.036
9. Li MM, Xu QJ, Han J et al (2015) Inhibition action and adsorption behavior of green inhibitor sodium carboxymethyl cellulose on copper. Int J Electrochem Sci 10:9028–9041
10. Sangeetha Y, Meenakshi S, Sairam Sundaram C (2016) Corrosion inhibition of aminated hydroxyl ethyl cellulose on mild steel in acidic condition. Carbohydr Polym 150:13–20. https://doi.org/10.1016/j.carbpol.2016.05.002
11. Solomon MM, Umoren SA, Udosoro II, Udoh AP (2010) Inhibitive and adsorption behaviour of carboxymethyl cellulose on mild steel corrosion in sulphuric acid solution. Corros Sci 52:1317–1325. https://doi.org/10.1016/j.corsci.2009.11.041
12. Umoren SA, AlAhmary AA, Gasem ZM, Solomon MM (2018) Evaluation of chitosan and carboxymethyl cellulose as ecofriendly corrosion inhibitors for steel. Int J Biol Macromol 117:1017–1028. https://doi.org/10.1016/j.ijbiomac.2018.06.014
13. Charitha BP, Rao P (2017) Starch as an ecofriendly green inhibitor for corrosion control of 6061-Al alloy. J Mater Environ Sci 8:78–89
14. Parveen M, Mobin M, Zehra S, Aslam R (2018) L-proline mixed with sodium benzoate as sustainable inhibitor for mild steel corrosion in 1M HCl: an experimental and theoretical approach. Sci Rep 8:1–18. https://doi.org/10.1038/s41598-018-24143-2
15. Zulhusni MDM, Othman NK, Lazim AM (2015) Enhancement of corrosion resistance of carbon steel by *Dioscorea hispida* starch in NaCl. AIP Conf Proc. https://doi.org/10.1063/1.4931277
16. Fares MM, Maayta AK, Al-Mustafa JA (2012) Corrosion inhibition of iota-carrageenan natural polymer on aluminum in presence of zwitterion mediator in HCl media. Corros Sci 65:223–230. https://doi.org/10.1016/j.corsci.2012.08.018
17. Khairou KS, Alfi AA, Mabrouk EM (2007) Natural polymers as corrosion inhibitors for aluminium and tin in acidic media. Mater Sci Res India 4:279–290. https://doi.org/10.13005/msri/040207
18. Jmiai A, El Ibrahimi B, Tara A et al (2018) Alginate biopolymer as green corrosion inhibitor for copper in 1 M hydrochloric acid: experimental and theoretical approaches. J Mol Struct 1157:408–417. https://doi.org/10.1016/j.molstruc.2017.12.060
19. Obot IB, Onyeachu IB, Kumar AM (2017) Sodium alginate: a promising biopolymer for corrosion protection of API X60 high strength carbon steel in saline medium. Carbohydr Polym 178:200–208. https://doi.org/10.1016/j.carbpol.2017.09.049
20. Mobin M, Ahmad I, Murmu M, Banerjee P, Aslam R (2023) Corrosion inhibiting properties of polysaccharide extracted from *Lepidium meyenii* root for mild steel in acidic medium: experimental, density functional theory, and Monte Carlo simulation studies. J Phys Chem Solids 179:111411
21. Sundaram RG, Vengatesh G, Sundaravadivelu M (2020) Surface morphological and quantum chemical studies of some expired drug molecules as potential corrosion inhibitors for mild steel in chloride medium. Surf Interfaces. https://doi.org/10.1016/j.surfin.2020.100841
22. Zakaria K, Abbas MA, Bedair MA (2022) Herbal expired drug bearing glycosides and polysaccharides moieties as green and cost-effective oilfield corrosion inhibitor: electrochemical and computational studies. J Mol Liq 352:118689
23. Kumar MNVR (2000) A review of chitin and chitosan applications. React Funct Polym 46:1–27
24. Vorster SW, Waanders FB, Geldenhuys AJ (2001) Corrosion inhibitor, pp 1–24, patent cooperation treaty, WO01/21854 A2, 29 March 2001
25. Verma C et al (2018) Chitosan-based green and sustainable corrosion inhibitors for carbon steel, vol 13. Intechopen, London. https://doi.org/10.5772/intechopen.74989
26. Menaka R, Subhashini S (2016) Chitosan Schiff base as ecofriendly inhibitor for mild steel corrosion in 1 M HCl. J Adhes Sci Technol 30:1622–1640. https://doi.org/10.1080/01694243.2016.1156382
27. Singh CD, Ansari KR, Sorour AA et al (2018) Thiosemicarbazide and thiocarbohydrazide functionalized chitosan as ecofriendly corrosion inhibitors for carbon steel in hydrochloric acid solution. Int J Biol Macromol 107:1747–1757. https://doi.org/10.1016/j.ijbiomac.2017.10.050
28. Kong P, Feng H, Chen N et al (2019) Polyaniline/chitosan as a corrosion inhibitor for mild steel in acidic medium. RSC Adv 9:9211–9217. https://doi.org/10.1039/c9ra00029a
29. Chauhan DS, Srivastava V, Joshi PG, Quraishi MA (2018) PEG cross-linked Chitosan: a biomacromolecule as corrosion inhibitor for sugar industry. Int J Ind Chem 9:363–377. https://doi.org/10.1007/s40090-018-0165-0
30. Erna M, Herdini H, Futra D (2019) Corrosion inhibition mechanism of mild steel by amylose-acetate/carboxymethyl chitosan composites in acidic media. Int J Chem Eng. https://doi.org/10.1155/2019/8514132
31. Jessima SJHM, Berisha A, Srikandan SS, Subhashini S (2020) Preparation, characterization, and evaluation of corrosion inhibition efficiency of sodium lauryl sulfate modified chitosan for

mild steel in the acid pickling process. J Mol Liq. https://doi.org/10.1016/j.molliq.2020.114382
32. Jessima SJHM, Subhashini S, Berisha A, Oral A, Srikandan SS (2021) Corrosion mitigation performance of disodium EDTA functionalized chitosan biomacromolecule—experimental and theoretical approach. Int J Biol Macromol 178:477–491
33. Zhang QH, Xu N, Jiang ZN, Liu HF, Zhang GA (2023) Chitosan derivatives as promising green corrosion inhibitors for carbon steel in acidic environment: inhibition performance and interfacial adsorption mechanism. J Colloid Interface Sci 640:1052–1067. https://doi.org/10.1016/j.jcis.2023.02.141
34. Dalhatu SN, Modu KA, Mahmoud AA et al (2023) L-arginine grafted chitosan as corrosion inhibitor for mild steel protection. Polymers. https://doi.org/10.3390/polym15020398
35. Mouaden KE, Chauhan DS, Quraishi MA, Bazzi L, Hilali M (2020) Cinnamaldehyde-modified chitosan as a bio-derived corrosion inhibitor for acid pickling of copper: microwave synthesis, experimental and computational study. Int J Biol Macromol 164:3709–3717. https://doi.org/10.1016/j.ijbiomac.2020.08.137
36. Lai X, Hu J, Ruan T et al (2021) Chitosan derivative corrosion inhibitor for aluminum alloy in sodium chloride solution : a green organic/inorganic hybrid. Carbohydr Polym 265:118074. https://doi.org/10.1016/j.carbpol.2021.118074
37. Mohamed RR, Fekry AM (2011) Antimicrobial and anticorrosive activity of adsorbents based on chitosan schiff's base. Int J Electrochem Sci 6:2488–2508
38. Sher VV, Voevoda NV (1969) Comparative study of the anti oxidant and anti corrosion properties of metal dialkyl and diaryldithiophosphates. Chem Technol Fuels Oils 5:305–307
39. Boujakhrout A, Hamdani I, Chahboun N, Bouyanzer A et al (2015) Antioxidant activity and corrosion inhibitive behavior of *Garcinia cola* seeds on mild steel in hydrochloric medium. J Mater Environ Sci 6:3655–3666
40. Hussin MH (2015) Antioxidant and anticorrosive properties of oil palm frond lignins extracted with different techniques. Ann For Sci 72:17–26. https://doi.org/10.1007/s13595-014-0405-1
41. Prabakaran M, Hemapriya V, Kim SH, Chung IM (2019) Evaluation of antioxidant and anticorrosion properties of *Epipremnum aureum*. Arab J Sci Eng 44:169–178. https://doi.org/10.1007/s13369-018-3398-5
42. Vorobyova VI, Skiba MI, Shakun AS, Nahirniak SV (2019) Relationship between the inhibition and antioxidant properties of the plant and biomass wastes extracts—a review. Int J Corros Scale Inhib 8:150–178. https://doi.org/10.17675/2305-6894-2019-8-2-1
43. Woranuch S, Yoksan R (2013) Preparation, characterization and antioxidant property of water-soluble ferulic acid grafted chitosan. Carbohydr Polym 96:495–502. https://doi.org/10.1016/j.carbpol.2013.04.006
44. Giuliani C, Pascucci M, Riccucci C et al (2018) Chitosan-based coatings for corrosion protection of copper-based alloys: a promising more sustainable approach for cultural heritage applications. Prog Org Coat 122:138–146. https://doi.org/10.1016/j.porgcoat.2018.05.002
45. American Society for Testing and Materials (2004) ASTM G1-03: Standard practice for preparing, cleaning, and evaluating corrosion test specimens. ASTM, Filadelfia, Pennsylvania
46. Jessima SJHM, Subhashini S, Arulraj J (2020) *Sunova spirulina* powder as an effective environmentally friendly corrosion inhibitor for mild steel in acid medium. J Bio- Tribo-Corros. https://doi.org/10.1007/s40735-020-00370-x
47. Berradja A (2019) Electrochemical techniques for corrosion and tribocorrosion monitoring: methods for the assessment of corrosion rates. IntechOpen, London
48. Chen S, Zhu B, Liang X (2020) Corrosion inhibition performance of coconut leaf extract as a green corrosion inhibitor for X65 steel in hydrochloric acid solution. Int J Electrochem Sci 15:1–15. https://doi.org/10.20964/2020.01.39
49. Guo L, El BY, Yu R et al (2020) Newly synthesized triazolopyrimidine derivative as an inhibitor for mild steel corrosion in HCl medium: an experimental and in silico study. J Mater Res Technol 9:6568–6578. https://doi.org/10.1016/j.jmrt.2020.04.044
50. Nazari MH, Shihab MS, Cao L et al (2017) A peony-leaves-derived liquid corrosion inhibitor: protecting carbon steel from NaCl. Green Chem Lett Rev 10:359–379. https://doi.org/10.1080/17518253.2017.1388446
51. Rosenbloom SN, Corbett RA (2007) An assessment of ASTM F 2129 electrochemical testing of small medical implants—lessons learned. In: NACE—International Corrosion Conference Series, pp 076741–0767410
52. Shahzad K, Sliem MH, Shakoor RA et al (2020) Electrochemical and thermodynamic study on the corrosion performance of API X120 steel in 3.5% NaCl solution. Sci Rep 10:1–15. https://doi.org/10.1038/s41598-020-61139-3
53. Wang D, Ramadan M, Kumseranee S et al (2020) Mitigating microbiologically influenced corrosion of an oilfield biofilm consortium on carbon steel in enriched hydrotest fluid using 2,2-dibromo-3-nitrilopropionamide (DBNPA) enhanced by a 14-mer peptide. J Mater Sci Technol 57:146–152. https://doi.org/10.1016/j.jmst.2020.02.087
54. Wyrwas RB, Lamothe ME (2013) Report on electrochemical corrosion testing of 241-SY-102 grab sampling campaign. Washington River Protection Solutions LLC, Richland
55. Yahya S, Othman NK, Daud AR, Jalar A (2014) Effect of scan rate on corrosion inhibition of carbon steel in the presence of rice straw extract—potentiodynamic studies. Sains Malays 43:1083–1087
56. Abd El-Wahab EA, Marei AH, Khalifa OR, Mohamed HA (2010) Corrosion behavior of aluminum electrode in absence and in presence of sodium chloride at different pH solutions using toludine as inhibitor. J Am Sci 6:476–486
57. Faiz M, Zahari A, Awang K, Hussin H (2020) Corrosion inhibition on mild steel in 1 M HCl solution by: *Cryptocarya nigra* extracts and three of its constituents (alkaloids). RSC Adv 10:6547–6562. https://doi.org/10.1039/c9ra05654h
58. Habeeb HJ, Luaibi HM, Abdullah TA et al (2018) Case study on thermal impact of novel corrosion inhibitor on mild steel. Case Stud Therm Eng 12:64–68. https://doi.org/10.1016/j.csite.2018.03.005
59. Manssouri M, Znini M, El Ouadi Y, Laghchimi A, Ouakki M, Majidi L (2020) Effect of aaronsohnia pubescens extracts to prevent against the corrosion of mild steel in 1.0 M HCl. Anal Bioanal Electrochem 12:944–958
60. Yan Y, Li W, Cai L, Hou B (2008) Electrochemical and quantum chemical study of purines as corrosion inhibitors for mild steel in 1 M HCl solution. Electrochim Acta 53:5953–5960. https://doi.org/10.1016/j.electacta.2008.03.065
61. Yilbas BS, Toor IH, Al-Sharafi A (2018) Anti-corrosive materials. In: Comprehensive energy systems. Elsevier, pp 913–943. https://doi.org/10.1016/B978-0-12-809597-3.00256-X
62. Jafar Mazumder MA (2019) Synthesis, characterization and electrochemical analysis of cysteine modified polymers for corrosion inhibition of mild steel in aqueous 1 M HCl. RSC Adv 9:4277–4294. https://doi.org/10.1039/c8ra09833f
63. Kartsonakis IA, Stamatogianni P, Karaxi EK, Charitidis CA (2020) Comparative study on the corrosion inhibitive effect of 2-mecraptobenzothiazole and Na_2HPO_4 on industrial conveying API 5L X42 pipeline steel. Appl Sci. https://doi.org/10.3390/app10010290

64. El B, Baddouh A, Oukhrib R et al (2021) Electrochemical and in silico investigations into the corrosion inhibition of cyclic amino acids on tin metal in the saline environment electrochemical and in silico investigations into the corrosion inhibition of cyclic amino acids on tin metal in the saline environment. Surf Interfaces 23:100966. https://doi.org/10.1016/j.surfin.2021.100966
65. El Faydy M, Benhiba F, Berisha A et al (2020) An experimental-coupled empirical investigation on the corrosion inhibitory action of 7-alkyl-8-hydroxyquinolines on C35E steel in HCl electrolyte. J Mol Liq 317:113973. https://doi.org/10.1016/j.molliq.2020.113973
66. Hsissou R, Benhiba F, Abbout S et al (2020) Trifunctional epoxy polymer as corrosion inhibition material for carbon steel in 1.0 M HCl: MD simulations, DFT and complexation computations. Inorg Chem Commun 115:107858. https://doi.org/10.1016/j.inoche.2020.107858
67. Hsissou R, Dagdag O, Abbout S et al (2019) Novel derivative epoxy resin TGETET as a corrosion inhibition of E24 carbon steel in 1.0 M HCl solution. Experimental and computational (DFT and MD simulations) methods. J Mol Liq 284:182–192. https://doi.org/10.1016/j.molliq.2019.03.180
68. Dagdag O, Hsissou R, El Harfi A, Berisha A, Safi Z, Verma C et al (2020) Fabrication of polymer based epoxy resin as effective anti-corrosive coating for steel: computational modeling reinforced experimental studies. Surf Interfaces. https://doi.org/10.1016/j.surfin.2020.100454
69. Dagdag O, Berisha A, Safi Z et al (2020) DGEBA-polyaminoamide as effective anti-corrosive material for 15CDV6 steel in NaCl medium: computational and experimental studies. J Appl Polym Sci 137:1–10. https://doi.org/10.1002/app.48402
70. Dagdag O, Hsissou R, El Harfi A, Safi Z, Berisha A, Verma C et al (2020) Epoxy resins and their zinc composites as novel anti-corrosive materials for copper in 3% sodium chloride solution: experimental and computational studies. J Mol Liq 315:113757. https://doi.org/10.1016/j.molliq.2020.113757
71. Abbout S, Zouarhi M, Chebabe D et al (2020) Galactomannan as a new bio-sourced corrosion inhibitor for iron in acidic media. Heliyon. https://doi.org/10.1016/j.heliyon.2020.e03574
72. Berisha A (2019) The influence of the grafted aryl groups on the solvation properties of the graphyne and graphdiyne—a MD study. Open Chem 17:703–710. https://doi.org/10.1515/chem-2019-0083
73. Dagdag O, Berisha A, Safi Z et al (2020) Highly durable macromolecular epoxy resin as anticorrosive coating material for carbon steel in 3% NaCl: computational supported experimental studies. J Appl Polym Sci. https://doi.org/10.1002/app.49003
74. Sun H, Jin Z, Yang C, Akkermans RL, Robertson SH, Spenley NA, Miller S, Todd SM (2016) COMPASS II: extended coverage for polymer and drug-like molecule databases. J Mol Model 22:1–10. https://doi.org/10.1007/s00894-016-2909-0
75. Rbaa M, Ouakki M, Galai M et al (2020) Simple preparation and characterization of novel 8-hydroxyquinoline derivatives as effective acid corrosion inhibitor for mild steel: experimental and theoretical studies. Colloids Surf A 602:125094. https://doi.org/10.1016/j.colsurfa.2020.125094
76. Queiroz MF, Melo KRT, Sabry DA et al (2015) Does the use of chitosan contribute to oxalate kidney stone formation? Mar Drugs 13:141–158. https://doi.org/10.3390/md13010141
77. Almeida RR, Silva Damasceno ET, de Carvalho SYB et al (2018) Chitosan nanogels condensed to ferulic acid for the essential oil of *Lippia origanoides* Kunth encapsulation. Carbohydr Polym 188:268–275. https://doi.org/10.1016/j.carbpol.2018.01.103
78. Li C, Li JB (2017) Preparation of chitosan-ferulic acid conjugate: structure characterization and in the application of pharmaceuticals. Int J Biol Macromol 105:1539–1543. https://doi.org/10.1016/j.ijbiomac.2017.04.103
79. Chatterjee NS, Anandan R, Navitha M et al (2016) Development of thiamine and pyridoxine loaded ferulic acid-grafted chitosan microspheres for dietary supplementation. J Food Sci Technol 53:551–560. https://doi.org/10.1007/s13197-015-2044-4
80. Liu J, Pu H, Liu S et al (2017) Synthesis, characterization, bioactivity and potential application of phenolic acid grafted chitosan: a review. Carbohydr Polym. https://doi.org/10.1016/j.carbpol.2017.07.014
81. Liu J, Wen XY, Lu JF, Kan J, Jin CH (2014) Free radical mediated grafting of chitosan with caffeic and ferulic acids: structures and antioxidant activity. Int J Biol Macromol 65:97–106. https://doi.org/10.1016/j.ijbiomac.2014.01.021
82. Elbasuney S, Gobara M, Zoriany M et al (2019) The significant role of stabilized colloidal ZrO_2 nanoparticles for corrosion protection of AA2024. Environ Nanotechnol Monit Manage. https://doi.org/10.1016/j.enmm.2019.100242
83. Rahman MM, Zahir H, Haq B, Al SDA (2018) Corrosion inhibition properties of waterborne poly urethane/cerium nitrate coatings on mild steel. Coatings. https://doi.org/10.3390/coatings8010034
84. Huffer S et al (2011) Anticorrosion pigments with positive zeta potential US 2011/0151266 A1. 1–7
85. Rugmini Ammal P, Prajila M, Joseph A (2018) Effective inhibition of mild steel corrosion in hydrochloric acid using EBIMOT, a 1, 3, 4-oxadiazole derivative bearing a 2-ethylbenzimidazole moiety: electro analytical, computational and kinetic studies. Egypt J Pet 27:823–833. https://doi.org/10.1016/j.ejpe.2017.12.004
86. Fathima A, Abdul S, Sethumanickam S (2017) Corrosion inhibition, adsorption and thermodynamic properties of poly (vinyl alcohol- cysteine) in molar HCl. Arab J Chem 10:S3358–S3366. https://doi.org/10.1016/j.arabjc.2014.01.016
87. Larabi L, Harek Y, Benali O, Ghalem S (2005) Hydrazide derivatives as corrosion inhibitors for mild steel in 1 M HCl. Progress Org Coat 54:256–262. https://doi.org/10.1016/j.porgcoat.2005.06.015
88. Zhang HH, Qin CK, Chen Y, Zhang Z (2019) Inhibition behaviour of mild steel by three new benzaldehyde thiosemicarbazone derivatives in 0.5 M H_2SO_4: experimental and computational study. R Soc Open Sci 6:190192. https://doi.org/10.1098/rsos.190192
89. Khadom AA, Yaro AS, Studies WL (2011) Protection of low carbon steel in phosphoric acid by potassium iodide. Prot Met Phys Chem Surf 47:662–669. https://doi.org/10.1134/S2070205111050078
90. Noor EA (2007) Temperature effects on the corrosion inhibition of mild steel in acidic solutions by aqueous extract of fenugreek leaves. Int J Electrochem Sci 2:996–1017
91. Singh A, Ituen EB, Ansari KR et al (2019) Surface protection of X80 steel using Epimedium extract and its iodide-modified composites in simulated acid wash solution: a greener approach towards corrosion inhibition. New J Chem 43:8527–8538. https://doi.org/10.1039/c9nj01691k
92. Arukalam IO, Madu IO, Ijomah NT et al (2014) Acid corrosion inhibition and adsorption behaviour of ethyl hydroxyethyl cellulose on mild steel corrosion. J Mater 2014:1–11. https://doi.org/10.1155/2014/101709
93. Karthikaiselvi R, Subhashini S (2014) Study of adsorption properties and inhibition of mild steel corrosion in hydrochloric acid media by water soluble composite poly (vinyl alcohol-o-methoxy aniline). J Assoc Arab Univ Basic Appl Sci 16:74–82. https://doi.org/10.1016/j.jaubas.2013.06.002
94. Singh A, Ansari KR, Quraishi MA, Lgaz H (2018) Effect of electron donating functional groups on corrosion inhibition of

J55 steel in a sweet corrosive environment: experimental, density functional theory, and molecular dynamic simulation. Materials (Basel). https://doi.org/10.3390/ma12010017
95. Eduok UM, Khaled M (2015) Corrosion inhibition for low-carbon steel in 1 M H_2SO_4 solution by phenytoin: evaluation of the inhibition potency of another "anticorrosive drug." Res Chem Intermed 41:6309–6324. https://doi.org/10.1007/s11164-014-1741-3
96. Roy P, Karfa P, Adhikari U, Sukul D (2014) Corrosion inhibition of mild steel in acidic medium by polyacrylamide grafted Guar gum with various grafting percentage: effect of intramolecular synergism. Corros Sci. https://doi.org/10.1016/j.corsci.2014.07.039
97. Xu X, Singh A, Sun Z, Ansari KR, Lin Y (2017) Theoretical, thermodynamic and electrochemical analysis of biotin drug as an impending corrosion inhibitor for mild steel in 15% hydrochloric acid. R Soc Open Sci. https://doi.org/10.1098/rsos.170933
98. Espinoza-Vázquez A, Rodríguez-Gómez FJ, Martínez-Cruz IK et al (2019) Adsorption and corrosion inhibition behaviour of new theophylline-triazole-based derivatives for steel in acidic medium. R Soc Open Sci. https://doi.org/10.1098/rsos.181738
99. Subramanian B, Maruthamuthu S, Rajan ST (2015) Biocompatibility evaluation of sputtered zirconium-based thin film metallic glass-coated steels. Int J Nanomed 10:17–29. https://doi.org/10.2147/IJN.S79977
100. Al-Amiery AA, Binti Kassim FA, Kadhum AAH, Mohamad AB (2016) Synthesis and characterization of a novel eco-friendly corrosion inhibition for mild steel in 1 M hydrochloric acid. Sci Rep 6:1–13. https://doi.org/10.1038/srep19890
101. Al-amiery AA, Othman MH, Adnan T et al (2018) Results in physics electrochemical studies of novel corrosion inhibitor for mild steel in 1 M hydrochloric acid. Results Phys 9:978–981. https://doi.org/10.1016/j.rinp.2018.04.004
102. Meeusen M, Zardet L, Homborg AM et al (2019) A complementary electrochemical approach for time-resolved evaluation of corrosion inhibitor performance. J Electrochem Soc 166:C3220–C3232. https://doi.org/10.1149/2.0271911jes
103. Kumar S, Vashisht H, Olasunkanmi LO et al (2016) Experimental and theoretical studies on inhibition of mild steel corrosion by some synthesized polyurethane tri-block co-polymers. Sci Rep 6:1–18. https://doi.org/10.1038/srep30937
104. Yildiz R (2015) An electrochemical and theoretical evaluation of 4,6-diamino-2-pyrimidinethiol as a corrosion inhibitor for mild steel in HCl solutions. Corros Sci 90:544–553. https://doi.org/10.1016/j.corsci.2014.10.047
105. Solmaz R (2014) Investigation of adsorption and corrosion inhibition of mild steel in hydrochloric acid solution by 5-(4-dimethylaminobenzylidene)rhodanine. Corros Sci 79:169–176. https://doi.org/10.1016/j.corsci.2013.11.001
106. Chakravarthy MP, Mohana KN (2014) Adsorption and corrosion inhibition characteristics of some nicotinamide derivatives on mild steel in hydrochloric acid solution. ISRN Corros 2014:1–13. https://doi.org/10.1155/2014/687276
107. Zavala Olivares G, Hernández Gayosso MJ, Mora Mendoza JL (2007) Corrosion inhibitors performance for mild steel in CO_2 containing solutions. Mater Corros 07730:427–437. https://doi.org/10.1002/maco.200604023
108. Xu S, Zhang S, Guo L, Feng L, Tan B (2019) Experimental and theoretical studies on the corrosion inhibition of carbon steel by two indazole derivatives in HCl medium. Materials (Basel) 12:1–11. https://doi.org/10.3390/ma12081339
109. Reddy CM, Sanketi BD, Narendra Kumar S (2016) Corrosion inhibition of mild steel by *Capsicum annuum* fruit paste. Perspect Sci 8:603–605. https://doi.org/10.1016/j.pisc.2016.06.033
110. Aslam R, Mobin M, Shoeb M, Murmu M, Banerjee P (2021) Proline nitrate ionic liquid as high temperature acid corrosion inhibitor for mild steel: experimental and molecular-level insights. J Ind Eng Chem 100:333–350
111. Babic M (2017) Role of interfacial chemistry on wettability and carbon dioxide corrosion of mild steels. http://rave.ohiolink.edu/etdc/view?acc_num=ohiou1483543296145156
112. Alamry KA, Khan A, Aslam J, Hussein MA, Aslam R (2023) Corrosion inhibition of mild steel in hydrochloric acid solution by the expired Ampicillin drug. Sci Rep. https://doi.org/10.1038/s41598-023-33519-y
113. Obot IB, Solomon MM, Onyeachu IB et al (2020) Development of a green corrosion inhibitor for use in acid cleaning of MSF desalination plant. Desalination 495:114675. https://doi.org/10.1016/j.desal.2020.114675
114. Hamdy A, El-Gendy NS (2013) Thermodynamic, adsorption and electrochemical studies for corrosion inhibition of carbon steel by henna extract in acid medium. Egypt J Pet 22:17–25. https://doi.org/10.1016/j.ejpe.2012.06.002
115. Wang C, Zou C, Cao Y (2021) Electrochemical and isothermal adsorption studies on corrosion inhibition performance of β-cyclodextrin grafted polyacrylamide for X80 steel in oil and gas production. J Mol Struct 1228:129737. https://doi.org/10.1016/j.molstruc.2020.129737
116. Sliem MH, Afifi M, Bahgat Radwan A et al (2019) AEO7 surfactant as an eco-friendly corrosion inhibitor for carbon steel in HCl solution. Sci Rep 9:1–16. https://doi.org/10.1038/s41598-018-37254-7
117. Shainy KM, Rugmini Ammal P, Unni KN et al (2016) Surface interaction and corrosion inhibition of mild steel in hydrochloric acid using pyoverdine, an eco-friendly bio-molecule. J Bio-Tribo-Corros 2:1–12. https://doi.org/10.1007/s40735-016-0050-3
118. Abboud Y, Abourriche A, Saffaj T et al (2007) 2,3-Quinoxalinedione as a novel corrosion inhibitor for mild steel in 1 M HCl. Mater Chem Phys 105:1–5. https://doi.org/10.1016/j.matchemphys.2007.03.037
119. Abdel-Gaber AM, Abd-El-Nabey BA, Sidahmed IM et al (2006) Inhibitive action of some plant extracts on the corrosion of steel in acidic media. Corros Sci 48:2765–2779. https://doi.org/10.1016/j.corsci.2005.09.017
120. Aloysius A, Ramanathan R, Christy A et al (2018) Experimental and theoretical studies on the corrosion inhibition of vitamins—thiamine hydrochloride or biotin in corrosion of mild steel in aqueous chloride environment. Egypt J Pet 27:371–381. https://doi.org/10.1016/j.ejpe.2017.06.003
121. Meng Y, Ning W, Xu B et al (2017) Inhibition of mild steel corrosion in hydrochloric acid using two novel pyridine Schiff base derivatives: a comparative study of experimental and theoretical results. RSC Adv 7:43014–43029. https://doi.org/10.1039/c7ra08170g
122. Mobin M, Aslam R, Salim R, Kaya S (2022) An investigation on the synthesis, characterization and anti-corrosion properties of choline based ionic liquids as novel and environmentally friendly inhibitors for mild steel corrosion in 5% HCl. J Colloid Interface Sci 620:293–312
123. El Ibrahimi B (2020) Atomic-scale investigation onto the inhibition process of three 1, 5- benzodiazepin-2-one derivatives against iron corrosion in acidic environment. Colloid Interface Sci Commun 37:100279. https://doi.org/10.1016/j.colcom.2020.100279
124. El Ibrahimi B, Soumoue A, Jmiai A et al (2016) Computational study of some triazole derivatives (un- and protonated forms) and their copper complexes in corrosion inhibition process. J Mol Struct. https://doi.org/10.1016/j.molstruc.2016.06.057
125. Zhang W, Li HJ, Wang M et al (2019) Highly effective inhibition of mild steel corrosion in HCl solution by using pyrido[1,2-a]benzimidazoles. New J Chem 43:413–426. https://doi.org/10.1039/C8NJ04028A

126. Xu Y, Zhang S, Li W et al (2018) Experimental and theoretical investigations of some pyrazolo-pyrimidine derivatives as corrosion inhibitors on copper in sulfuric acid solution. Appl Surf Sci 459:612–620. https://doi.org/10.1016/j.apsusc.2018.08.037
127. Fouda AS, Ismail MA, Abousalem AS, Elewady GY (2017) Experimental and theoretical studies on corrosion inhibition of 4-amidinophenyl-2,2′-bifuran and its analogues in acidic media. RSC Adv 7:46414–46430. https://doi.org/10.1039/c7ra08092a
128. Gece G (2015) Corrosion inhibition behavior of two quinoline chalcones: insights from density functional theory. Corros Rev 33:195–202. https://doi.org/10.1515/corrrev-2015-0028
129. Malekmohammadi Nouri P, Attar MM (2015) Experimental and quantum chemical studies on corrosion inhibition performance of fluconazole in hydrochloric acid solution. Bull Mater Sci 38:499–509. https://doi.org/10.1007/s12034-015-0865-4
130. Dagdag O, Hsissou R, Berisha A et al (2019) Polymeric-based epoxy cured with a polyaminoamide as an anticorrosive coating for aluminum 2024–T3 surface: experimental studies supported by computational modeling. J Bio- Tribo-Corros 5:1–13. https://doi.org/10.1007/s40735-019-0251-7
131. El Arrouji S, Karrouchi K, Berisha A et al (2020) New pyrazole derivatives as effective corrosion inhibitors on steel-electrolyte interface in 1 M HCl: electrochemical, surface morphological (SEM) and computational analysis. Colloids Surf A. https://doi.org/10.1016/j.colsurfa.2020.125325
132. Hsissou R, Abbout S, Berisha A et al (2019) Experimental, DFT and molecular dynamics simulation on the inhibition performance of the DGDCBA epoxy polymer against the corrosion of the E24 carbon steel in 1.0 M HCl solution. J Mol Struct 1182:340–351. https://doi.org/10.1016/j.molstruc.2018.12.030
133. Hsissou R, Abbout S, Seghiri R et al (2020) Evaluation of corrosion inhibition performance of phosphorus polymer for carbon steel in [1 M] HCl: computational studies (DFT, MC and MD simulations). J Mater Res Technol. https://doi.org/10.1016/j.jmrt.2020.01.002
134. Mehmeti VV, Berisha AR (2017) Corrosion study of mild steel in aqueous sulfuric acid solution using 4-methyl-4h-1,2,4-triazole-3-thiol and 2-mercaptonicotinic acid-an experimental and theoretical study. Front Chem. https://doi.org/10.3389/fchem.2017.00061
135. Rbaa M, Dohare P, Berisha A et al (2020) New epoxy sugar based glucose derivatives as eco friendly corrosion inhibitors for the carbon steel in 1.0 M HCl: experimental and theoretical investigations. J Alloys Compd 833:154949. https://doi.org/10.1016/j.jallcom.2020.154949
136. Thaçi V, Hoti R, Berisha A, Bogdanov J (2020) Corrosion study of copper in aqueous sulfuric acid solution in the presence of (2E,5E)-2,5-dibenzylidenecyclopentanone and (2E,5E)-bis[(4-dimethylamino)benzylidene]cyclopentanone: experimental and theoretical study. Open Chem 18:1412–1420. https://doi.org/10.1515/chem-2020-0172
137. Ibrahimi BE, Bazzi L, Issami SE (2020) The role of pH in corrosion inhibition of tin using the proline amino acid : theoretical and experimental investigations. RSC Adv 10:29696–29704. https://doi.org/10.1039/d0ra04333h
138. Oukhrib R, El B, Abou H et al (2020) In silico investigations of alginate biopolymer on the Fe (110), Cu (111), Al (111) and Sn (001) surfaces in acidic media: quantum chemical and molecular mechanic calculations. J Mol Liq 312:113479. https://doi.org/10.1016/j.molliq.2020.113479
139. Berisha A (2020) Experimental, Monte Carlo and molecular dynamic study on corrosion inhibition of mild steel by pyridine derivatives in aqueous perchloric acid. Electrochem 1:188–199. https://doi.org/10.3390/electrochem1020013
140. Hsissou R, Benzidia B, Rehioui M et al (2020) Anticorrosive property of hexafunctional epoxy polymer HGTMDAE for E24 carbon steel corrosion in 1.0 M HCl: gravimetric, electrochemical, surface morphology and molecular dynamic simulations. Polym Bull 77:3577–3601. https://doi.org/10.1007/s00289-019-02934-5
141. Umoren SA, Solomon MM, Saji VS (2022) Polymeric materials in corrosion inhibition fundamentals and applications, 1st edn. Elsevier, Amsterdam
142. Kokalj A (2022) Corrosion inhibitors: physisorbed or chemisorbed? Corros Sci 196:109939
143. Umoren SA, Banera MJ, Alonso-Garcia T et al (2013) Inhibition of mild steel corrosion in HCl solution using chitosan. Cellulose 20:2529–2545. https://doi.org/10.1007/s10570-013-0021-5
144. Rabizadeh T, Khameneh Asl S (2018) Chitosan as a green inhibitor for mild steel corrosion: thermodynamic and electrochemical evaluations. Mater Corros 70:1–11. https://doi.org/10.1002/maco.201810501
145. Gupta NK, Joshi PG, Srivastava V, Quraishi MA (2018) Chitosan: a macromolecule as green corrosion inhibitor for mild steel in sulfamic acid useful for sugar industry. Int J Biol Macromol 106:704–711. https://doi.org/10.1016/j.ijbiomac.2017.08.064
146. Solomon MM, Gerengi H, Kaya T, Umoren SA (2017) Performance evaluation of a chitosan/silver nanoparticles composite on St37 steel corrosion in a 15% HCl solution. ACS Sustain Chem Eng 5:809–820. https://doi.org/10.1016/j.ijbiomac.2017.06.072
147. Solomon MM, Gerengi H, Umoren SA (2017) Carboxymethyl cellulose/silver nanoparticles composite: synthesis, characterization and application as a benign corrosion inhibitor for St37 steel in 15% H_2SO_4 medium. ACS Appl Mater Interfaces 9:6376–6389. https://doi.org/10.1021/acsami.6b14153
148. Okoronkwo AE, Olusegun SJ, Oluwasina OO (2015) The inhibitive action of chitosan extracted from Archachatina marginata shells on the corrosion of plain carbon steel in acid media. Anti-Corros Methods Mater 1:13–18. https://doi.org/10.1108/ACMM-10-2013-1307
149. Akbarzadeh E, Ibrahim MNM, Rahim AA et al (2013) Monomers of lignin as corrosion inhibitors for mild steel: study of their behaviour by factorial experimental design. Corros Eng Sci Technol. https://doi.org/10.1179/1743278212Y.0000000013
150. Akbarzadeh E, Ibrahim MNM, Rahim AA (2011) Corrosion inhibition of mild steel in near neutral solution by kraft and soda lignins extracted from oil palm empty fruit bunch. Int J Electrochem Sci 6:5396–5416
151. Marina AJL, De Gois JS, Toaldo IM et al (2020) Optimization of espresso spent ground coffee waste extract preparation and the influence of its chemical composition as an eco-friendly corrosion inhibitor for carbon steel in acid medium. Mater Res 23:1–12
152. Shen M, Furman A, Kharshan R (2015) Investigation of bio-based aromatic acids as corrosion inhibitor. In: NACE international corrosion and conference Expo 2015, pp 1–12
153. Arash S, Alibakhshi E, Bahlakeh G (2019) A detailed atomic level computational and electrochemical exploration of the *Juglans regia* green fruit shell extract as a sustainable and highly ef fi cient green corrosion inhibitor for mild steel in 3. 5 wt % NaCl solution. J Mol Liq 284:682–699. https://doi.org/10.1016/j.molliq.2019.04.045
154. Chung I, Malathy R, Kim S et al (2020) Ecofriendly green inhibitor from Hemerocallis fulva against aluminum corrosion in sulphuric acid medium. J Adhes Sci Technol. https://doi.org/10.1080/01694243.2020.1712770
155. Begum AAS, Vahith RMA, Kotra V et al (2021) Spilanthes acmella leaves extract for corrosion inhibition in acid medium. Coatings 11:1–24. https://doi.org/10.3390/coatings11010106

156. Gupta DK, Awasthi L, Das AK et al (2020) Corrosion inhibition effect of acidic extract of bark of eucalyptus globulus on mild steel. Tribhuvan Univ J 35:1–10. https://doi.org/10.3126/tuj.v35i1.35828
157. Zaher A, Chaouiki A, Salghi R et al (2020) Inhibition of mild steel corrosion in 1M hydrochloric medium by the methanolic extract of Ammi visnaga L. Lam seeds. Int J Corros. https://doi.org/10.1155/2020/9764206
158. Sanaei Z, Ramezanzadeh M, Bahlakeh G, Ramezanzadeh B (2019) Use of Rosa canina fruit extract as a green corrosion inhibitor for mild steel in 1 M HCl solution: a complementary experimental, molecular dynamics and quantum mechanics investigation. J Ind Eng Chem 69:18–31. https://doi.org/10.1016/j.jiec.2018.09.013
159. Lgaz H, Masroor S, Chafiq M et al (2020) Evaluation of 2-mercaptobenzimidazole derivatives as corrosion inhibitors for mild steel in hydrochloric acid. Metals (Basel) 10:357
160. Caldona EB, Zhang M, Liang G et al (2021) Corrosion inhibition of mild steel in acidic medium by simple azole-based aromatic compounds. J Electroanal Chem 880:114858. https://doi.org/10.1016/j.jelechem.2020.114858
161. Salman TA, Jawad QA, Hussain MAM et al (2020) New environmental friendly corrosion inhibitor of mild steel in hydrochloric acid solution: adsorption and thermal studies. Cogent Eng 7. https://doi.org/10.1080/23311916.2020.1826077
162. Elsharif AM, Abubshait SA, Abdulazeez I, Abubshait HA (2020) Synthesis of a new class of corrosion inhibitors derived from natural fatty acid: 13-Docosenoic acid amide derivatives for oil and gas industry. Arab J Chem 13:5363–5376. https://doi.org/10.1016/j.arabjc.2020.03.015
163. Sehmi A, Ouici HB, Guendouzi A et al (2020) Corrosion inhibition of mild steel by newly synthesized pyrazole carboxamide derivatives in HCl acid medium: experimental and theoretical studies. J Electrochem Soc 167:155508. https://doi.org/10.1149/1945-7111/abab25
164. Haque J, Srivastava V, Chauhan DS et al (2018) Microwave-induced synthesis of chitosan schiff bases and their application as novel and green corrosion inhibitors: experimental and theoretical approach. ACS Omega 3:5654–5668. https://doi.org/10.1021/acsomega.8b00455

Authors and Affiliations

S. J. Hepziba Magie Jessima[1] · S. Subhashini[2] · Avni Berisha[3] · Valbonë Mehmeti[4] · Subramanian Sathy Srikandan[5]

✉ S. J. Hepziba Magie Jessima
hepziba.magie@christuniversity.in

[1] Department of Chemistry, CHRIST (Deemed to be University), Bengaluru 560029, India

[2] Department of Chemistry, Avinashilingam Institute for Home Science and Higher Education for Women (Deemed to be University), Coimbatore 641043, India

[3] Chemistry Department of Natural Sciences Faculty, University of Prishtina, rr. "NënaTereze" nr.5, Prishtina 10000, Kosovo

[4] Materials Science - Nanochemistry Research Group, NanoAlb – Unit of Albanian Nanoscience and Nanotechnology, 10000 Tirana, Albania

[5] Department of Applied Science, PSG College of Technology, Coimbatore 641004, India